

Simulation of the planktonic ecosystem response to pre- and post-1976 forcing in an isopycnic model of the North Pacific

S.P. Haigh, K.L. Denman, and W.W. Hsieh

Abstract: To investigate the hypothesis that the 1976 “regime shift” in North Pacific fish populations resulted from climatic change propagating up the fisheries food web, we have embedded a four-component planktonic ecosystem model in an ocean general circulation model. The Miami isopycnic model (MICOM) has been implemented on a 2° grid over the domain from 18°S to 61°N, with a Kraus–Turner-type mixed layer model overlaying 10 isopycnal layers. An initial baseline run with forcing for the period 1952–1988 reasonably reproduces the spatial patterns and seasonal changes in SeaWiFS images. Estimates of annual net and export production compare well with contemporary observations of primary and export production at Ocean Station Papa in the subarctic North Pacific but are low by a factor of 8–10 at station ALOHA near Hawaii. Two subsequent runs with forcing for the periods 1952–1975 and 1977–1988 show the main gyres to strengthen after 1976 with large areas of increased mixed layer depth. In the light-limited subarctic, limited areas of shallower spring mixed layer produced increased phytoplankton biomass, whereas in the nutrient-limited subtropical gyre, increased nutrients (or migration of the subarctic front and the equatorial current system into the gyre) after 1976 correlated with increased plankton biomass.

Résumé : Pour évaluer l’hypothèse selon laquelle le « changement de régime » observé en 1976 chez les populations de poissons du Pacifique Nord est dû à une modification du climat qui s’est répercutée à travers la chaîne alimentaire jusqu’aux poissons, nous avons incorporé un modèle écosystémique du plancton à quatre compartiments à un modèle général de circulation océanique. Le modèle isopycnique de Miami (MICOM) a été appliqué à une grille ayant une résolution de 2° et couvrant un domaine de calcul allant de 18°S à 61°N, avec une modélisation de la couche de mélange de type Kraus–Turner superposant 10 couches isopycniques. Un premier passage du modèle avec forçage pour la période 1952–1988 a généré des patterns spatiaux et des changements saisonniers qui correspondent de façon satisfaisante aux images des capteurs SeaWiFS. Les estimations des productions annuelles nette et exportée se comparent avantageusement aux observations récentes des productions primaire et exportée à la « Ocean Station Papa » dans le Pacifique Nord subarctique, mais elles sont trop basses par un facteur de 8–10 à la station ALOHA près d’Hawaii. Deux passages subséquents du modèle avec forçage pour les périodes de 1952–1975 et de 1977–1988 montrent un renforcement des tourbillons océaniques après 1976, ainsi que la présence de grandes surfaces où la profondeur de la couche de mélange s’est accrue. Dans la région subarctique où la lumière est le facteur limitant, les zones réduites de couches de mélange peu profondes au printemps ont produit des biomasses accrues de phytoplancton; en revanche, dans le tourbillon subtropical où les nutriments sont le facteur limitant, une augmentation des nutriments (ou la migration dans le tourbillon subtropical du front subarctique et du système du courant équatorial) après 1976 est en corrélation avec une croissance de la biomasse du plancton.

[Traduit par la Rédaction]

Introduction

There is currently broad interest in understanding how climate change affects marine fish populations. A changing climate affects fish populations in two ways: directly through, for example, temperature changes on physiology and larval survival or currents affecting migration pathways and larval

settlement, and indirectly by altering the production and dynamics of the marine planktonic ecosystem that supplies the food energy required by fish. In this paper, we focus on the second pathway: how the marine ecosystem responds to a change in climate.

Around 1976, a major climate shift occurred in and over the North Pacific Ocean: the Aleutian atmospheric low pres-

Received March 8, 2000. Accepted October 18, 2000. Published on the NRC Research Press Web site on March 16, 2001. J15656

S.P. Haigh. Institute of Ocean Sciences, P.O. Box 6000, Sidney, BC V8L 4B2, Canada, and Department of Earth and Ocean Sciences, University of British Columbia, Vancouver, BC V6T 1Z4, Canada.

K.L. Denman.¹ Canadian Centre for Climate Modelling and Analysis, University of Victoria, P.O. Box 1700, Victoria, BC V8W 2Y2, Canada, and Institute of Ocean Sciences, P.O. Box 6000, Sidney, BC V8L 4B2, Canada.

W.W. Hsieh. Department of Earth and Ocean Sciences, University of British Columbia, Vancouver, BC V6T 1Z4, Canada.

¹Corresponding author (Canadian Centre for Climate Modelling and Analyses) (e-mail: ken.denman@ec.gc.ca).

sure system strengthened and shifted its characteristic position, with correlated changes in sea surface temperature (SST) and wind patterns (Hanawa et al. 1989; Trenberth and Hurrell 1994; Nakamura et al. 1997). This "regime shift" lasted from about 1976 until 1988 and was characterized by an intensification and southward shift of the winter Aleutian low pressure system. This shift transported warmer air northward along the west coast of North America and over Alaska, causing an increase in SST along the west coast of North America and Alaska. The intensification and southward shift of the winter Aleutian low pressure system correlates with a decrease in SST over the central subarctic North Pacific especially associated with the subarctic front (Nakamura et al. 1997). There were also stronger zonal winds over the central North Pacific and a cyclonic rotation of wind stress to a more poleward direction in the Gulf of Alaska. Miller and Schneider (2000) have recently analyzed the 1976 climate shift in terms of multidecadal climate dynamics in the North Pacific Ocean.

A number of biological changes appear to have been associated with the 1976 regime shift. In the eastern subarctic Pacific, changes in the ocean temperatures and currents correlate with changes in the migration patterns of fish (Mysak 1986). Venrick et al. (1987) observed an increase in chlorophyll *a* concentrations in the central North Pacific since the late 1970s and attributed this change to the increase in winter winds and the decrease in surface temperature. Brodeur and Ware (1992) found a doubling of summer zooplankton biomass in the subarctic Pacific between the periods 1952–1962 and 1980–1989. However, analysis of long-term time series by Sugimoto and Tadokoro (1997) did not yield marked changes in zooplankton or phytoplankton time series in the western subarctic that could be related to the changes in climate forcing that occurred around 1976. Beamish (1993), Francis et al. (1998), and Beamish et al. (1999) documented changes in fish populations associated with large-scale changes in atmospheric pressure patterns, including those observed around 1976.

To study how North Pacific planktonic ecosystems might respond to future changes in the climate, we use a coupled physical–biological model to simulate the ecosystem changes associated with the coupled atmosphere–ocean changes around 1976. We employ a three-dimensional ocean general circulation model (OGCM) with an embedded planktonic ecosystem model implemented over a domain from 18°S to the Bering Strait (61°N) on a nominal 2° grid with realistic bottom topography. The area of interest is the midlatitude North Pacific. The tropics have been included to make the southern boundary of the domain well removed from the area of interest. The model is run with monthly wind forcing and SSTs. Monthly average salinities were used in an initial run for the period 1952–1988, but annual average salinity fields were used in the simulations described next. We report on the results of three simulations: (i) a "baseline" run with mean forcing for the period 1952–1989, (ii) a "pre-1976" run with mean forcing for the period 1952–1975, and (iii) a "post-1976" run with mean forcing for the period 1977–1989. We analyze these simulations in the context of available observations on planktonic ecosystems in the subarctic and subtropical gyres.

Model description

OGCM

We use the Miami isopycnic coordinate ocean model (MICOM) as described by Bleck et al. (1992). Rather than grid points at constant depths, an isopycnic or layered model has a number of constant density layers whose position and thickness change at each horizontal gridpoint each time step. MICOM includes an explicit representation of the mixed layer, making it suitable for ecosystem modelling. The model employs the diapycnal mixing formulation of McDougall and Dewar (1998), whereby vertical exchanges depend on the concept of two-way entrainment of fluid across each interface. Conventional diffusion coefficients cannot be used in an isopycnic model because the net fluxes of heat, salt, and fluid volume into each layer must be specified so as to maintain the constant density of the layer.

We have implemented MICOM for the North Pacific Ocean with a model domain from 18°S to 61°N and bathymetry developed from the ETOPO5 data set smoothed with a 1–2–1 filter in both horizontal directions. A no-slip condition was used for the velocity fields at all lateral boundaries. In addition, the southern boundary was represented by a solid insulated vertical wall. The model has a coarse resolution Mercator grid of $2^\circ \times (2 \cos \varphi)^\circ$ with 11 layers in the vertical: a Kraus–Turner-type mixed layer and 10 isopycnic layers with potential density values of 24.16, 25.60, 26.15, 26.38, 26.60, 26.96, 27.24, 27.45, 27.60, and 27.70, chosen to have reasonable resolution of the upper few hundred metres north of approximately 35°N. The temperature and salinity fields were initialized with the World Ocean Atlas (1994) (WOA94) September data set. The circulation model was initialized on 1 September, when the mixed layer is at its shallowest in extratropical regions, because in MICOM, mixed layer deepening is better represented than mixed layer shallowing.

Surface forcing of the model used the current Comprehensive Ocean–Atmosphere Data Set (COADS) (e.g., Woodruff et al. 1987), which calculates separate monthly means for the wind stress (and its curl) and the wind speed, which was used in the calculation of mixed layer depth. We restored surface conditions to the observed SST and salinity with a time scale of 1 month for a mixed layer depth of 50 m. For wind speed, wind stress, and SST, three monthly climatologies were created from for the periods 1952–1988, 1952–1975, and 1977–1988 to obtain first a long-term mean annual cycle and then pre- and post-1976 mean annual cycles. Wind stress was calculated from the standard expression

$$[\tau_x, \tau_y] = \rho C_d V [u, v]$$

where the drag coefficient C_d is calculated from the expressions of Trenberth et al. (1989) and Large and Pond (1981), ρ is the density of air, V is wind speed at a height of 10 m, and $[u, v]$ are the vector components of V .

We examined the World Ocean Database (1998) (WOD98, Levitus et al. 1998) and concluded that there are insufficient data to create different monthly sea surface salinity climatologies for the pre- and post-1976 periods. Instead, annual mean salinity fields were created from WOD98 for the three periods listed above. Two model runs were carried out over

the 1952–1988 period to examine the effect of using annual mean (versus monthly mean) sea surface salinity to force the model. The first run used the 1952–1988 monthly climatologies for wind speed, wind stress, and SST and the monthly climatology for sea surface salinity from WOA94. The second run was identical to the first except that we averaged sea surface salinity (from WOA94) over 12 months to give an annual average salinity field. Minor differences in spatial patterns of mixed layer depths were observed, but results of the ecosystem model showed little change. Subsequently, we used the annual sea surface salinity fields in all simulations described here, and monthly SST fields throughout.

The climatologies for wind speed, SST, and salinity were smoothed using the same spatial filter as for the topography. The physical model was started from rest and spun up for 30.5 years using 1952–1988 climatologies, prior to embedding the ecosystem model described next.

Ecosystem model

The ecosystem model consists of four compartments, nutrient N , phytoplankton P , zooplankton Z , and detritus D , where nitrogen is the “currency” used (i.e., all four variables have units of millimoles nitrogen per cubic metre). For a complete description and equations of the NPZD model, see Denman and Peña (1999). Here, we describe only differences from their model.

The NPZD model described by Denman and Peña (1999) was used to examine the possible effects of iron limitation at Ocean Station Papa (OSP). As there is not sufficient knowledge of the role of iron over the entire North Pacific Ocean, we did not include the effect of iron limitation here, i.e., their iron limitation factor L_{Fe} was set equal to 1. Denman and Peña (1999) also used a light function derived from Webb et al. (1974). For numerical efficiency and since we do not resolve diurnal cycles in our coarse-resolution model, we calculate a daily averaged phytoplankton growth rate using the formulation of Evans and Parslow (1985) for the daily growth rate of phytoplankton as a function of light.

To model light shading by phytoplankton P and detritus D , Denman and Peña (1999) modified the linear formulation of the light attenuation coefficient used by Evans and Parslow (1985) and Fasham (1995). Compared with the vertical resolution of the one-dimensional model of Denman and Peña (1999) (60 layers over 120 m), our physical model has a coarse vertical resolution: 11 layers over the entire depth of the ocean, which is inadequate for resolving the shading effects of phytoplankton and detritus. Thus, we did not include feedback from the biomass to light attenuation and used the same linear formulation as Evans and Parslow (1985) and Fasham (1995).

MICOM has 12 months with equal length of 30 days, resulting in a 360-day year. Since formulation of the daily irradiance field is based on a 365-day year (Iqbal 1983), modifications were necessary so that the ecosystem model could be run for a 360-day year. We assumed that the 360-day year has the same number of hours per year as the 365-day year, resulting in $(365 \times 24)/360 = 73/3$ h per day. The irradiance field was modified by assuming that the amount of light per day is $(73/3)/24 = 73/72$ times the amount per day

for a 365-day year, equivalent to modifying the solar constant by a factor of $73/72$. In addition, the day angle was defined as $2\pi(t - 1)/360$, where $t = 1, \dots, 360$. Calculating the total amount of light in a year for this formulation gives an error of less than 1 part in 10^9 when compared with that of Iqbal (1983) for the 365-day year.

Denman and Peña (1999) used a linear zooplankton loss term, which because of the nature of the coupled differential equations results in essentially no seasonal cycle in the phytoplankton field. This choice is apparently justified when modelling the annual cycle at OSP where there is no seasonal cycle in the observed chlorophyll concentrations. However, satellite images do show that there are regions in the North Pacific Ocean where well-defined seasonal cycles in surface chlorophyll are present. In addition, recent unpublished measurements (K.L. Denman and M.A. Peña, personal communication) indicate that the chlorophyll to nitrogen ratio in the phytoplankton at OSP may have an annual cycle as inferred from laboratory and modelling studies by Goericke and Montoya (1998). Thus, although there is no annual cycle in the observed phytoplankton chlorophyll at OSP, we might expect to see a seasonal cycle in phytoplankton biomass P , measured as either nitrogen (the currency of our model) or carbon. For these reasons, we chose to use a quadratic zooplankton loss term, which allows a seasonal cycle in the phytoplankton biomass field (expressed as nitrogen) in the vicinity of OSP and elsewhere.

We assumed that the biological parameters are constant in time and space and used the parameter values given by Denman and Peña (1999) with the following exceptions. For the zooplankton grazing half-saturation constant, zooplankton losses to nutrients, and zooplankton losses to detritus, we used the values from Denman et al. (1998) for their model run with a quadratic zooplankton mortality term. In addition, the maximum phytoplankton growth rate was reduced from 2.0 to 1.0-day^{-1} . As this model does not include iron limitation, using a value of 2.0-day^{-1} gave a depletion of surface nutrients in the subarctic Northeast Pacific Ocean in the summer months, contrary to observations, which generally show that the subarctic Northeast Pacific Ocean is a high-nutrient, low-chlorophyll (HNLC) region. Reducing the maximum phytoplankton growth rate to 1.0-day^{-1} gives the desired behavior when iron limitation is absent in the model. As in Denman and Peña (1999) and Denman et al. (1998), the maximum grazing rate has been set to be representative of microzooplankton and the tight grazing control they seem to exert in a wide variety of oceanic regimes (e.g., Landry et al. 1997).

Coupled model

Embedding the NPZD model into MICOM was based on the methods of Drange (1994), who embedded a carbon cycle model into a North Atlantic implementation of MICOM. Although we used a different ecosystem model that does not include an inorganic carbon cycle module, the embedding structure is essentially the same.

As the OGCM has coarse vertical resolution, primary production below the mixed layer could be underestimated if the mixed layer depth is much shallower than the euphotic zone depth. Gross primary production over a time step is

equal to the biomass of phytoplankton P times the rate of primary production times the time step. If the layer immediately below the mixed layer is several hundred metres thick, then the biomass will be mixed over those several hundred metres each time step; if the layer below the mixed layer is much thinner, then the biomass will be mixed over a much smaller depth range and its average value will be higher. In the latter case, the primary production will be greater where there is light (below the mixed layer but still within the euphotic zone) because the biomass concentration P will be greater. In reality, the layers below the mixed layer are not subjected to high rates of vertical mixing, making this dependency of primary production on the thickness of the layer immediately below the mixed layer an artifact of the vertical resolution of the model. To minimize this effect, we split the physical layers at 100 m. This separated the model domain into a thin productive surface zone (above 100 m), which is exposed to higher light levels and a deep zone where light levels are very low and no production is allowed. It should be noted that the 100-m level is an arbitrary choice, as the actual euphotic zone depth based on the 1% light level is 78 m for the parameter values used. In the revised model, if the mixed layer depth was greater than 100 m, the two sublayers were remixed after calculation of the biological source/sink terms. If the mixed layer depth was less than 100 m, the split at the 100-m level was maintained within the biological model and NPZD were diffused across this level. As in Drange (1994), a definition based on turbulence theory (Gaspar et al. 1990) was used for the diffusion coefficient $K_v = k/N \text{ m}^2 \cdot \text{s}^{-1}$ where N is the buoyancy frequency and $k = 10^{-7} \text{ m}^2 \cdot \text{s}^{-2}$ (Gargett 1984). We imposed bounding limits of $10^{-6} < K_v < 10^{-1} \text{ m}^2 \cdot \text{s}^{-1}$ and used the mass-conserving implementation of diffusion in a nonuniform grid, both as described by Drange (1994).

MICOM's advection scheme (Bleck et al. 1992) was applied to the advection of NPZD by the velocity field. Advection and horizontal diffusion of the ecosystem components as well as the effects of diapycnal mixing and mixed layer shoaling/deepening on the concentration of the ecosystem variables were calculated once a day. Biological source/sink terms were computed five times a day with a forward Euler time-stepping scheme.

The coupled model was initiated with the results from the 30.5-year spinup for the physical fields. We used the annual nitrate field from WOA94 to initialize the nitrogen compartment. The other compartments (phytoplankton, zooplankton, and detritus) were initialized with a small concentration ($0.1 \text{ mmol N} \cdot \text{m}^{-3}$) in the mixed layer and zero concentration below the mixed layer. The ecosystem model was started on 1 March when the mixed layer is deepest and biological standing stocks in the North Pacific Ocean should be lowest. Experience from the one-dimensional ecosystem model (Denman and Peña 1999) indicates that the spinup time is less than 6 months, although it appears to take the three-dimensional model 2 years to come to equilibrium (see Results and discussion), probably because of the additional effects of horizontal fluxes.

As with the forcing fields for the physical model, there are three climatologies for cloud cover modulating surface solar irradiance that drives primary production. These fields are derived from COADS data for the periods 1952–1988,

1952–1975, and 1977–1988 and have been smoothed. We performed three different model runs of 5 years: (i) with 1952–1988 climatologies (baseline run), (ii) with 1952–1975 climatologies (pre-1976 run), and (iii) with 1977–1988 climatologies (post-1976 run).

Results and discussion

The first part of this section examines results for the annual cycle of the biological fields of the baseline run. The second part examines the impact of the 1976 regime shift on biological production by comparing the results from the pre- and post-1976 runs.

Baseline run

Nitrogen budget

The total budget of nitrogen from all four compartments should be conserved, since there are no imposed sources or sinks: Fig. 1a indicates a small loss of nitrogen (less than $0.1\% \cdot \text{year}^{-1}$) due to numerical errors. When embedding an ecosystem model into a physical model, parameter values must be carefully selected such that the nitrogen sinking out of the surface layer in the form of detritus balances the physical resupply of nutrients to the surface layer, averaged over the annual cycle and over the model domain. We chose to leave parameter values for the physical model unchanged and adjusted those of the ecosystem model. The amount of nitrogen in the top 100 m is sensitive to the remineralization length scale w_s/r_e where w_s is the detrital sinking rate and r_e is the remineralization rate. After several "tuning" runs, values of $w_s = 3 \text{ m} \cdot \text{day}^{-1}$ and $r_e = 0.1 \cdot \text{day}^{-1}$ were chosen. After 2 years of acclimation, the total amount of nitrogen in the top 100 m approaches equilibrium, changing less than $1\% \cdot \text{year}^{-1}$ (Fig. 1b). Thus, all results shown are from the third year of the coupled model run. The redistribution of nitrogen in the top 100 m due to horizontal transports fails to equilibrate after 5 years, and total nitrogen north of the equator is being lost at a rate of approximately $3\% \cdot \text{year}^{-1}$. This redistribution also occurs, to a lesser extent, at depth (Fig. 1c). We believe that this redistribution is due, at least in part, to the boundary conditions. Specifically, by closing off the Bering Strait, the Sea of Okhotsk, the Sea of Japan, the Arafura Sea, the eastern connections with the Indian Ocean from the Philippines through to New Guinea, and the southern boundary along 18°S (treated as a solid wall), it is likely that we have reduced supplies of nutrients to the surface layer north of the equator.

Surface distributions

To determine how well the model performs, we compare surface concentrations of the biological fields with available data. We start by examining the mixed layer concentration of N and comparing it with the annual concentration of nitrate from WOA94 averaged over the model's annually averaged mixed layer depth (Fig. 2). Although there are some differences, the model reproduces the major features of the observed nitrate distribution, in particular the subarctic front with high concentrations of N in the subpolar gyre and low concentrations of N in the subtropical gyre. Concentrations of modelled N in the subpolar gyre are slightly lower than

observed, probably resulting from the net loss of N north of the equator. At the equator, there is a band of high N concentrations from equatorial upwelling, in agreement with WOA94. However, the band is narrower than observed, which we believe results from phytoplankton using up more N in the model than in observations, as discussed in detail below. Finally, there is a buildup of surface N in southeast corner of the model domain, which probably is caused by the imposed southern boundary that, at present, is a solid wall. In eastern boundary currents, there is usually a subsurface poleward transport of nutrient-rich water caused by an undercurrent associated with wind-driven coastal or shelf edge upwelling. In the model, the solid boundary at 18°S prevents this transport towards the south. Thus, in the model, much of the enhanced N that is produced by remineralization of sinking detritus below the highly productive waters off Ecuador and Peru reappears at the surface due to wind-driven coastal upwelling rather than being transported southward (poleward) by the undercurrent. North of the equator, enhanced N transported northward in the model by the (unobstructed) poleward undercurrent supports elevated primary production and surface P along the coast of North America between 25 and 40°N (see Figs. 3a and 4).

We compare the seasonal cycle of surface phytoplankton biomass P with SeaWiFS imagery, where the SeaWiFS data have been converted from chlorophyll to nitrogen using the following relationship: $0.3 \text{ mmol N}\cdot\text{m}^{-3} \approx 0.4 \text{ mg Chl}\cdot\text{m}^{-3}$ based on $\text{C}:\text{Chl} = 60$ (g:g) and a Redfield ratio for $\text{C}:\text{N}$ of 6.6 (mol:mol) (Fig. 3). It is worth noting that the surface concentration of P produced by the model is the same as the mixed layer concentration of P . Satellite color images, however, estimate chlorophyll concentrations that are heavily weighted towards concentrations in the top few metres because of the approximately exponential decay of irradiance with depth. This difference in averaging depth may account for some of the differences observed where the SeaWiFS data appear to give much higher concentrations of P than the model, especially if the model produces (in low-wind conditions) a summer mixed layer that is too deep. Sugimoto and Tadokoro (1997) estimated the mean horizontal distribution of chlorophyll concentration north of 35°N from transparency depth. The levels are higher than those from either the model or the SeaWiFS imagery, and the horizontal patterns are considerably more patchy than either, possibly because in any given year, the transparency observations would have been sparse and concentrated along particular cruise tracks.

The location of the transition zone chlorophyll front (the southern extent of the subarctic high biomass region) migrates seasonally both in model results and in satellite observations, although the modelled front may extend further south than the observed front. In the subarctic gyre, phytoplankton biomass (expressed as nitrogen) undergoes a seasonal cycle in both model results and observations. Surface P maxima in the subarctic gyre occur during the summer in the model results and in the fall (December 1997 – November 1998) in the SeaWiFS data. However, the 1990s have been the warmest on record and 1998 was an anomalous year. During 1998, the equatorial Pacific evolved from a period of strong El Niño conditions to La Niña conditions by the end of the year. Thus, the average forcing fields based on 1952–1988 data may not be representative of the 1990s and

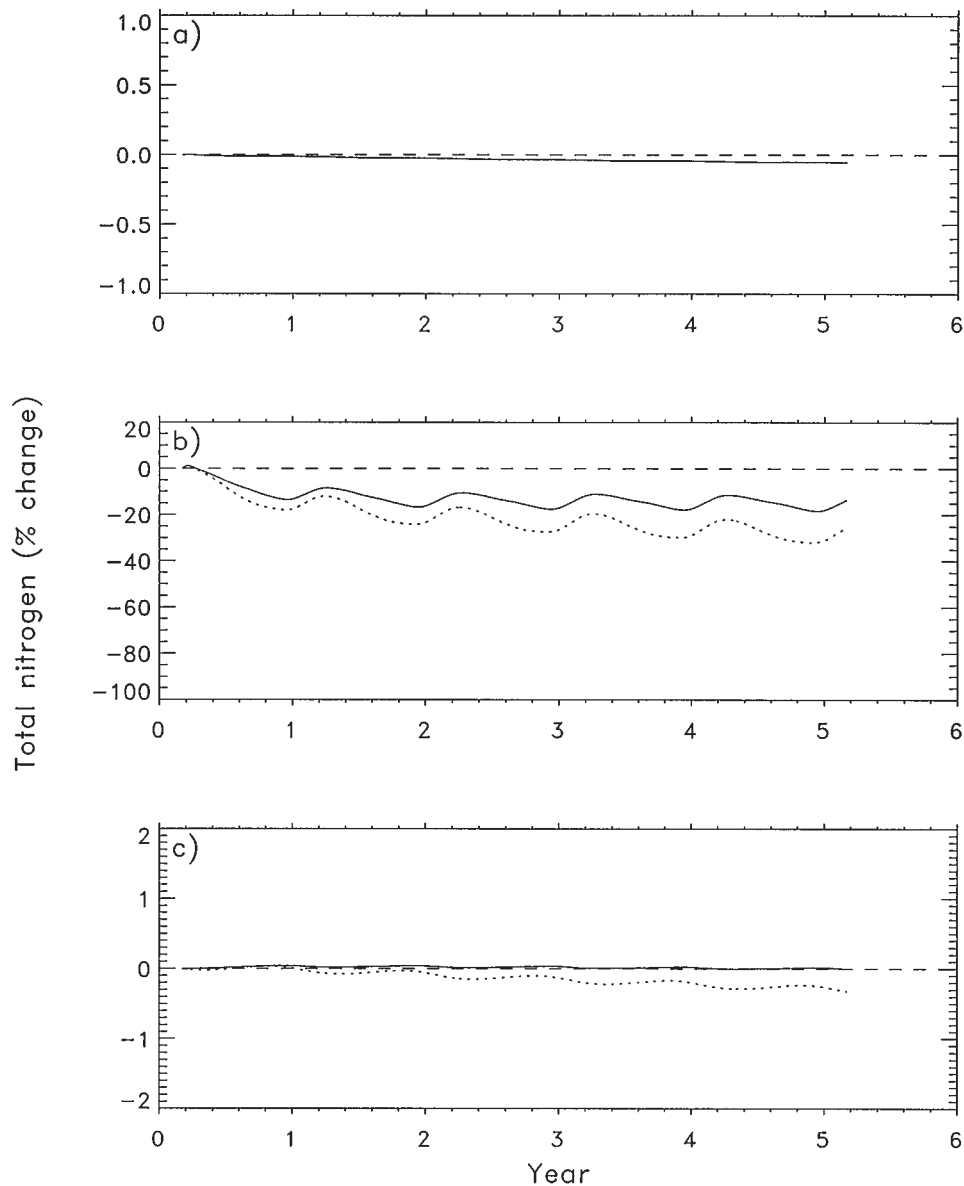
of 1998 in particular, the warmest year recorded globally. Comparing SeaWiFS data from the period October–November 1997 with those of October–November 1998, values in the fall of 1997 appear to be lower. In the subtropical gyre, surface concentrations of phytoplankton biomass are low in both model results and observations, due to low surface nutrient concentrations. The model reproduces the band of high biomass observed at the equator, although in the model, the band has little seasonal variation whereas SeaWiFS data indicate a significant seasonal cycle. Once again, we attribute this difference to the observation that 1998 was a year in transition from El Niño to La Niña conditions. CZCS images, based on data from November 1978 – June 1986, show little seasonal variation of chlorophyll at the equator. The band of P along the equator in the model results is also wider than in satellite images. It is believed that the surface equatorial region is an HNLC region deficient in iron (e.g., Landry et al. 1997), such that any iron present is used up near the equator. The surface water that diverges away from the equator then has been stripped of iron, limiting P growth, although it may still contain sufficient nitrate for growth, resulting in a narrow band of phytoplankton chlorophyll and a wider band of nitrate along the equator. In the model, we do not include iron limitation: the phytoplankton continue to use N away from the equator, resulting in a wider band of P and a narrower band of N than observed.

The seasonal cycle of modelled mixed layer microzooplankton Z follows closely that of P . Modelled time series at a given station show that there is a lag in Z , but this lag is too short to show up in the seasonal averages. Because there exist insufficient observations to compare basin plots of zooplankton concentrations, we do not show plots of surface Z . However, we have compared the seasonal cycle of Z at OSP with S. Strom's field data (Western Washington University, Bellingham, Wash., personal communication; Strom et al. 1993). In the model results, Z is high in the summer and low in the winter whereas the field data suggest the opposite behavior. Our model does not include mesozooplankton, which graze on the microzooplankton and large diatoms. In the winter at OSP, most copepods are dormant in "diapause" well below the surface and do not graze on the microzooplankton. Thus, in the subarctic gyre, copepods may reduce the number of microzooplankton in the summer but have little effect on winter population levels, which could explain differences in observed and modelled microzooplankton concentrations.

Primary production and vertical fluxes

The amount of energy available to higher trophic levels, fish and humans, and the amount of carbon dioxide fixed into organic molecules are functions of primary production, not just of population concentrations. The spatial distribution of annual primary production (moles nitrogen per square metre per year) in the third year of the coupled simulation (Fig. 4) basically reflects the summer pattern in phytoplankton biomass P shown in Fig. 3a. There are few well-sampled estimates of annual primary production in the North Pacific. The best sampled is that based on historical Secchi disk observations of water transparency where Falkowski and Wilson (1992) used empirical relationships to convert transparency depth to chlorophyll biomass to primary pro-

Fig. 1. Budget of total nitrogen ($N + P + Z + D$) in the (a) entire basin, (b) surface 100 m, and (c) below 100 m. In Figs. 1b and 1c, the solid line represents the budget over the entire basin and the dotted line represents the budget north of the equator.



duction rate, each step being subject to large uncertainty. Nevertheless, from 10 733 observations over forty $10 \times 10^\circ$ boxes north of the equator, they estimated an average chlorophyll concentration of $0.33 \pm 0.31 \text{ mg}\cdot\text{m}^{-3}$ and an average annual primary production of $189 \pm 85 \text{ g C}\cdot\text{m}^{-2}\cdot\text{year}^{-1}$. For comparison with primary production estimates based on ^{14}C -uptake studies, the highest value on the color scale in Fig. 4, $5 \text{ mol N}\cdot\text{m}^{-2}\cdot\text{year}^{-1}$, corresponds to $396 \text{ g C}\cdot\text{m}^{-2}\cdot\text{year}^{-1}$ (assuming a Redfield ratio C:N of 6.6 (mol:mol)). It would appear that the average over Fig. 4 north of the equator would be below the estimate of Falkowski and Wilson (1992).

There have been two sites where long-term observational programs have allowed more direct estimates of annual primary production, usually based on many ^{14}C -uptake experiments: OSP at 50°N , 145°W in the subarctic gyre and the Hawaiian Ocean Timeseries (HOT) station ALOHA at

$22^\circ45'\text{N}$, 158°W in the subtropical gyre. Before comparing estimates, we should point out that there continues to be controversy about what ^{14}C -uptake studies measure. Our ecological model does not explicitly include respiration of phytoplankton, so the nutrient uptake term is a reasonable analogue to the primary production estimated from ^{14}C -uptake experiments. Several contemporary estimates from OSP lie in the range $170\text{--}215 \text{ g C}\cdot\text{m}^{-2}\cdot\text{year}^{-1}$. From Fig. 4, the model-based estimate of annual primary production at OSP is about $2.65 \text{ mol N}\cdot\text{m}^{-2}\cdot\text{year}^{-1}$, or about $210 \text{ g C}\cdot\text{m}^{-2}\cdot\text{year}^{-1}$, in the center of the observed range, not entirely surprising, since our ecosystem model and parameter values originated from a one-dimensional model developed for OSP but without iron limitation (Denman and Peña 1999). The model also estimates similar levels of annual primary production in the western subarctic gyre, in agreement with

Fig. 2. Annually averaged mixed layer concentration of nutrient N ($\text{mmol N}\cdot\text{m}^{-3}$). (a) Nitrate from WOA94; (b) from model with 1952–1988 forcing: baseline run.

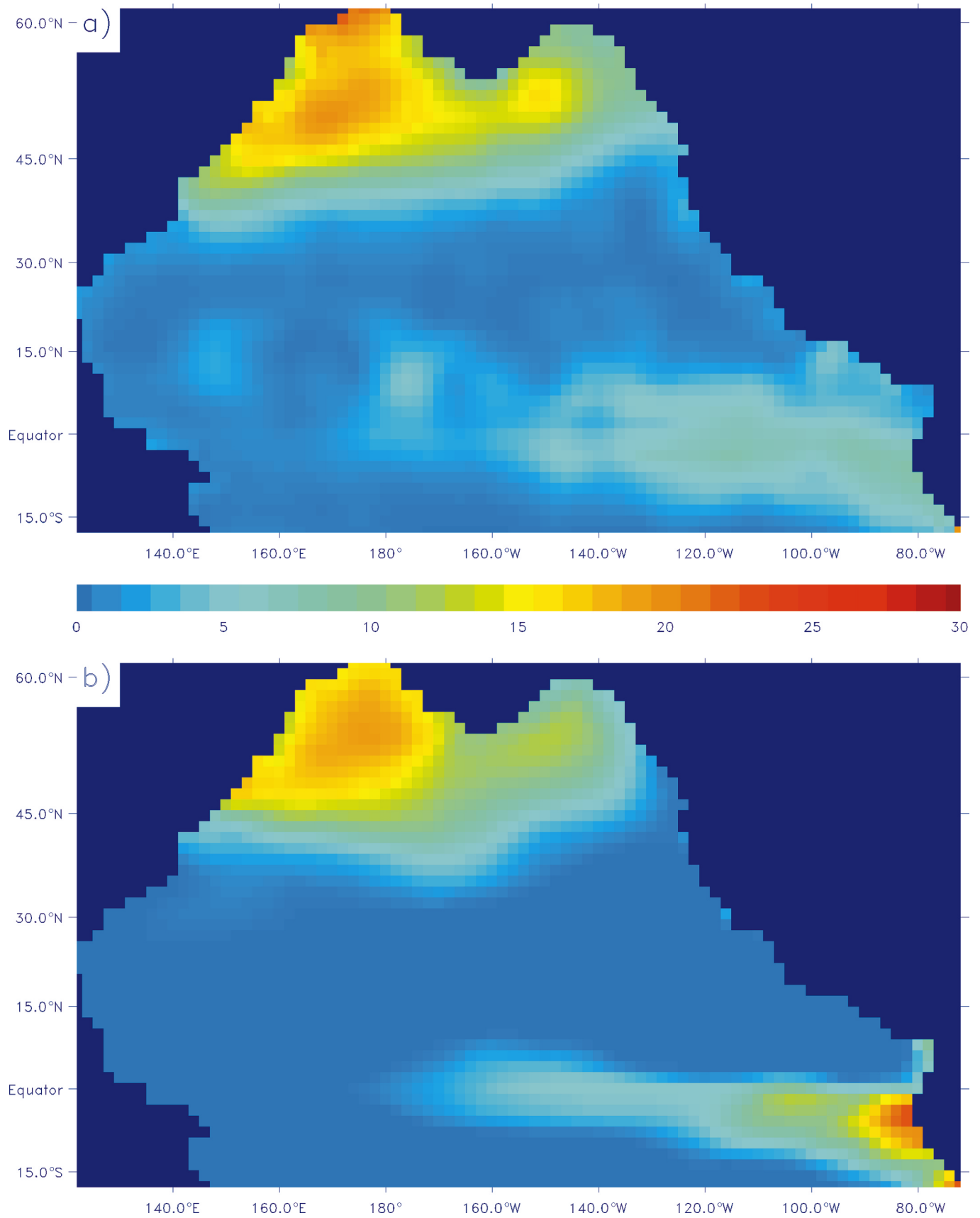
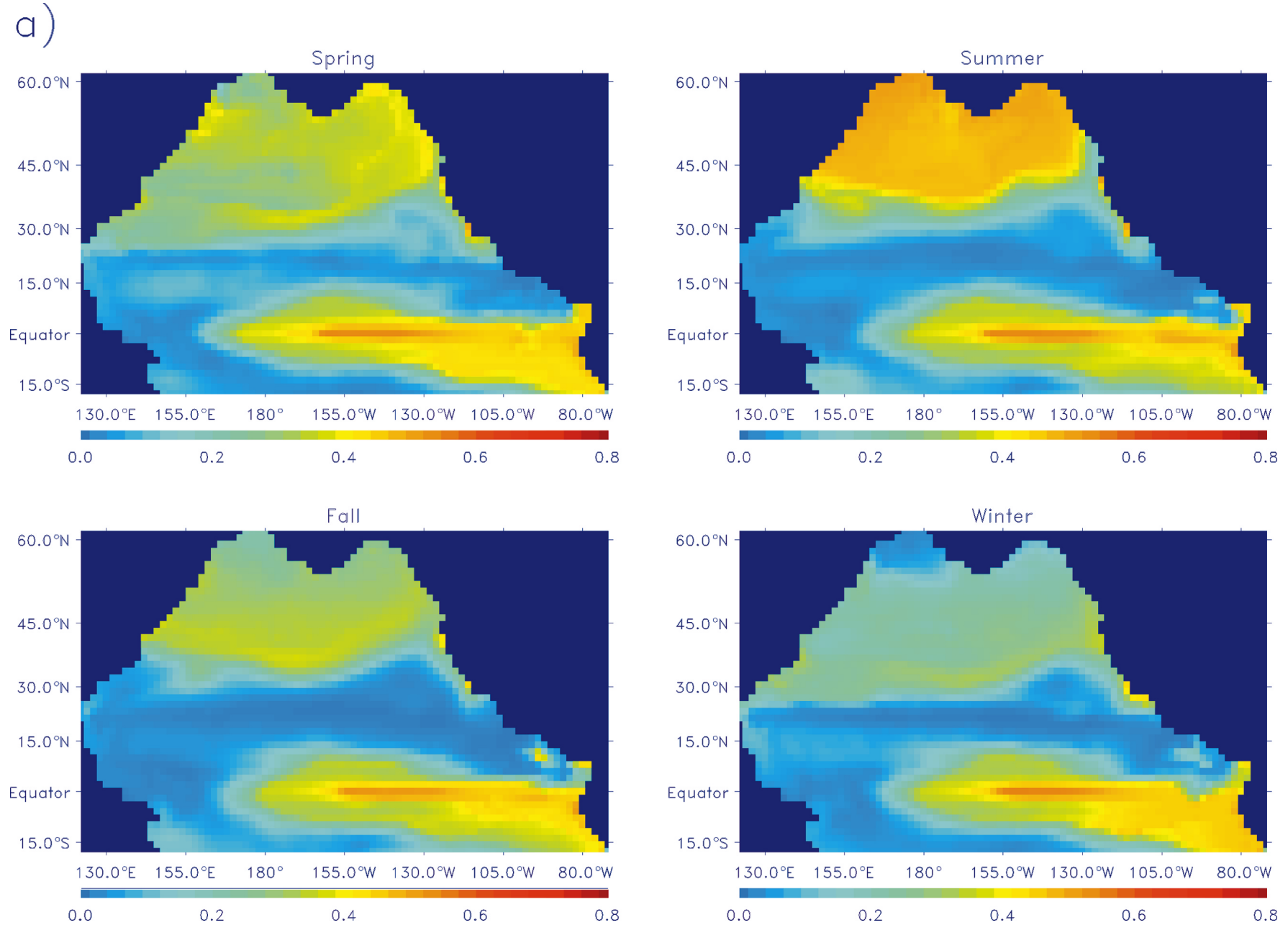
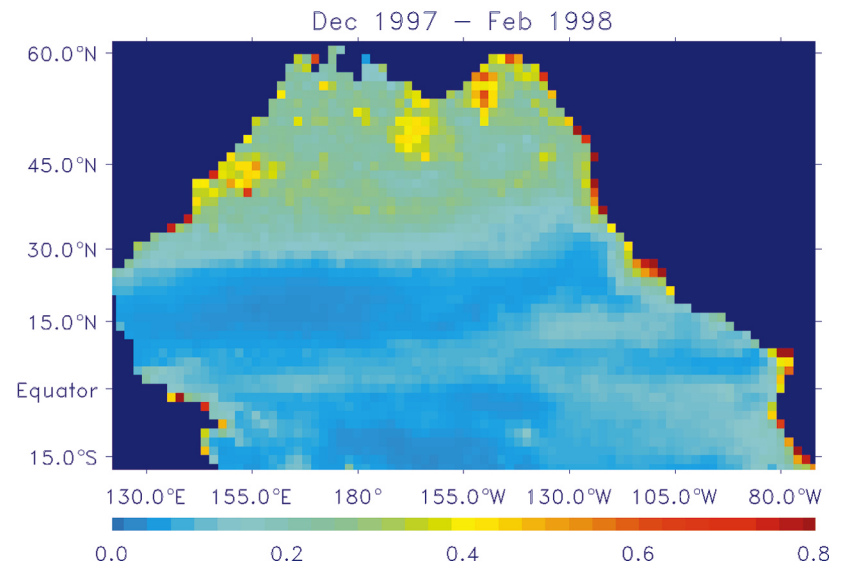
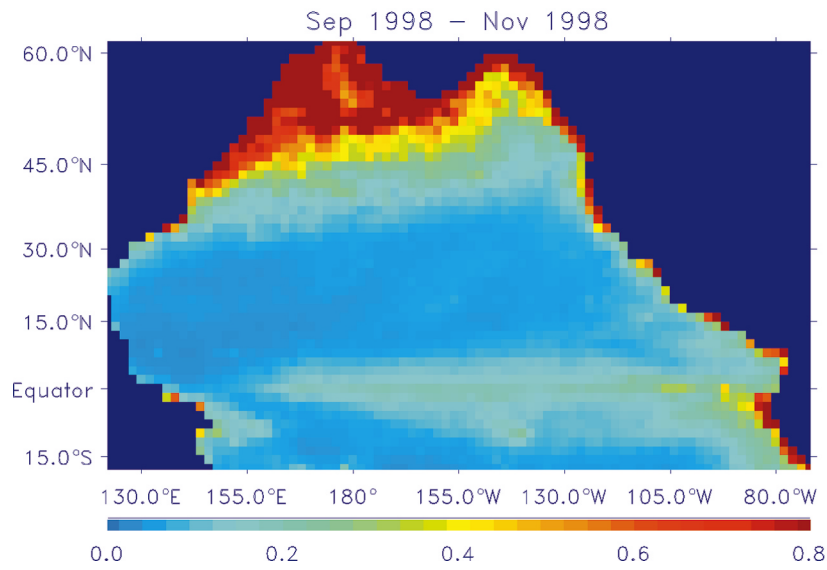
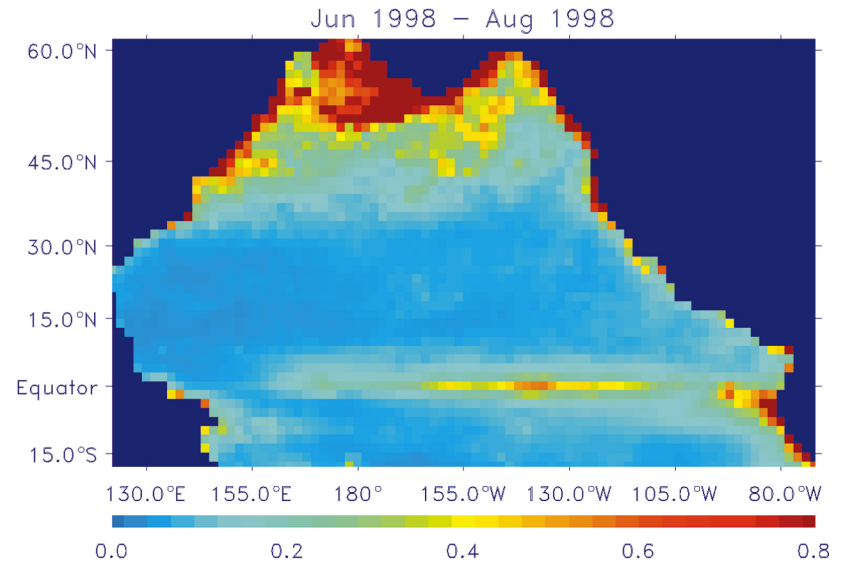
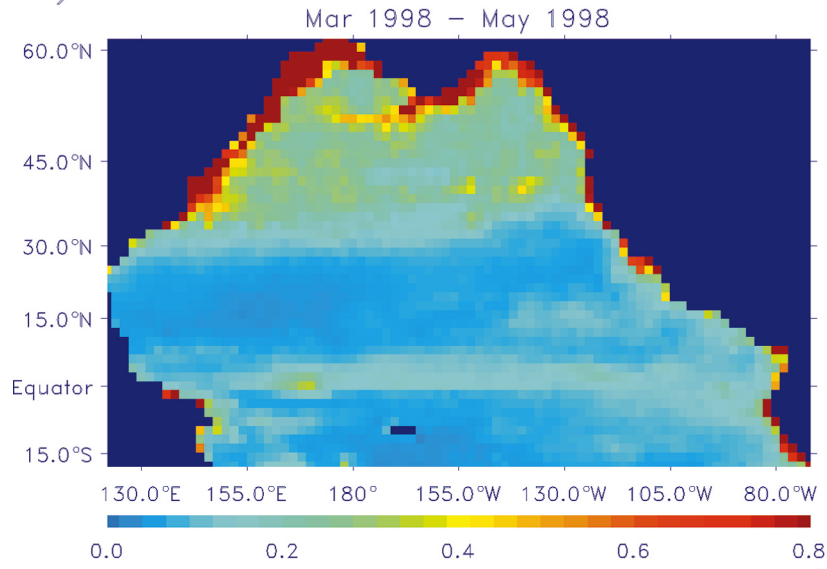


Fig. 3. Seasonally averaged concentration of phytoplankton P ($\text{mmol N}\cdot\text{m}^{-3}$) for spring (March–May), summer (June–August), fall (September–November), and winter (December–February) (a) in the mixed layer from the 1952–1988 baseline run and (b) near the surface from SeaWiFS imagery (from estimated chlorophyll a) for the year December 1997 – November 1998. To be consistent with Fig. 1a, winter (December 1997 – February 1998) was placed last, even though it leads the other seasons in time.



b)



observations compiled by Harrison et al. (1999, their table 2) showing similar summertime levels of primary production in both the western and the eastern subarctic.

The estimate of annual primary production at ALOHA is about $0.11 \text{ mol N}\cdot\text{m}^{-2}\cdot\text{year}^{-1}$, or about $9 \text{ g C}\cdot\text{m}^{-2}\cdot\text{year}^{-1}$ (Fig. 4). From 70 ^{14}C -uptake experiments over the period from October 1988 to July 1997, Karl et al. (1998) estimated the mean primary production at ALOHA to be $472 \text{ mg C}\cdot\text{m}^{-2}\cdot\text{day}^{-1} = 172 \text{ g C}\cdot\text{m}^{-2}\cdot\text{year}^{-1}$. They argued that this estimate is too high by about 30% when compared with estimates based on different filters but that when dissolved organic carbon production is included, the value may be two to three times higher. Even taking their lowest estimate, about 70% of $172 \text{ g C}\cdot\text{m}^{-2}\cdot\text{year}^{-1}$, to be about $120 \text{ g C}\cdot\text{m}^{-2}\cdot\text{year}^{-1}$, our model estimate for ALOHA is more than 10 times lower. It has been argued that there might be an "island effect" elevating primary production at ALOHA, but few would argue that it would increase the rate by a factor of 10.

In the context both of carbon cycling and planktonic production available to higher trophic levels, the export production is a key quantity. This export production must be supported by a net supply of N into the sunlit euphotic layer: from below, from the atmosphere, or from riverine input. In Fig. 5a, we show the net upward flux of N across the 100-m level from all sources of mixing and advection in the model. There is a large input in the area of the Kuroshio and Oyashio currents and in the central subarctic. Analysis of the individual contributing terms (not shown) indicates that vertical mixing dominates only in the Kuroshio–Oyashio region, probably from entrainment as the mixed layer deepens in the autumn and winter, reaching maximum depths greater than 175 m compared with winter maxima around 100 m in the eastern subarctic. There are areas of net downward flux of N (inside the closed contours) in the western equatorial region and east of 160°W in the subequatorial regions.

As there are no harvested trophic levels in our model, the downward flux of organic nitrogen across the 100-m level is exactly the export production. Most of the export production is in the form of sinking particles D , but for completeness, we show in Fig. 5b the annual downward flux of $P + Z + D$. In an equilibrium bounded ocean (without riverine or atmospheric nitrogen inputs), this downward flux (averaged over an annual cycle and the areal domain of the model) should exactly balance the upward flux across 100 m of dissolved inorganic nitrogen N , shown in Fig. 5a. (Recall from Fig. 1 that they do balance within a fraction of a percent of the total nitrogen in the model.)

There are no reliable measurement-based estimates of the annual upward flux of dissolved inorganic nitrogen. Instead, we again compare the model estimates of the downward flux of organic nitrogen at a depth of 100 m with observation-based estimates of export production at OSP and ALOHA. Because of the controversy surrounding estimates based on particles captured in sediment traps, we will compare with estimates based on chemical mass balances made by the same investigators at both sites. At ALOHA, the model estimate of export production (Fig. 5b) is less than $0.04 \text{ mol N}\cdot\text{m}^{-2}\cdot\text{year}^{-1} = 3 \text{ g C}\cdot\text{m}^{-2}\cdot\text{year}^{-1}$. The estimate for several years in the early 1990s is $2.0 \pm 0.9 \text{ mol C}\cdot\text{m}^{-2}\cdot\text{year}^{-1} = 24 \text{ g C}\cdot\text{m}^{-2}\cdot\text{year}^{-1}$ (Emerson et al. 1997), i.e., about eight times the model estimate. At OSP, the model estimate is about

$0.28 \text{ mol N}\cdot\text{m}^{-2}\cdot\text{year}^{-1} = 22 \text{ g C}\cdot\text{m}^{-2}\cdot\text{year}^{-1}$. The estimate based on oxygen budgets based on observations taken over several years is about $140 \text{ mg C}\cdot\text{m}^{-2}\cdot\text{day}^{-1} = 50 \text{ g C}\cdot\text{m}^{-2}\cdot\text{year}^{-1}$ (Emerson et al. 1991), about two times the model estimate. From a mean estimate of annual primary production at OSP (based on ^{14}C -uptake experiments) of $200 \text{ g C}\cdot\text{m}^{-2}\cdot\text{year}^{-1}$ (Harrison et al. 1999) and an f ratio based on nitrogen-uptake studies of 0.21–0.29 (Varela and Harrison 1999), we can estimate export production (taking it equivalent to new production) to be 42–58 $\text{g C}\cdot\text{m}^{-2}\cdot\text{year}^{-1}$, equivalent to the estimate of Emerson et al. (1991). Bearing in mind that most of the observational estimates of annual primary production and export production have uncertainties of the order $\pm 50\%$, our model estimates at OSP are within the uncertainties but biased low. However, the model estimates at ALOHA are between eight and 10 times lower than the best estimates based on observations.

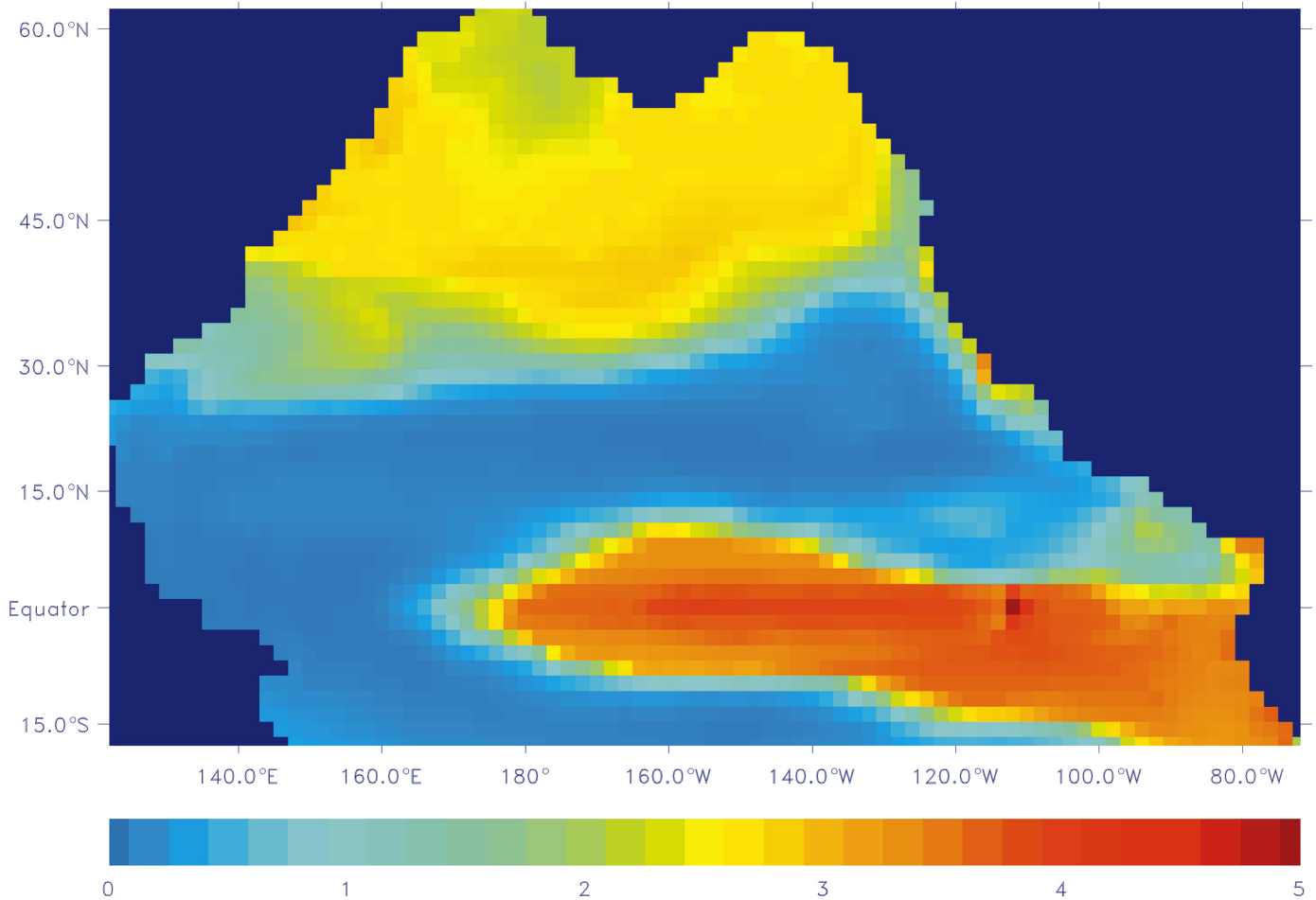
If all grid points in the model were in a one-dimensional balance over the annual cycle, then the two panels of Fig. 5 would be identical. They are not identical and differ appreciably in the equatorial Pacific and in the region associated with the Kuroshio current. In these regions, horizontal advection of the biological quantities significantly affects the local balance above 100 m. In addition, on time scales shorter than a year, horizontal fluxes may dominate the local balance in certain regions, especially when periods of upward flux of nutrient and of downward export of organic material are widely separated during the year. Moreover, a one-dimensional balance everywhere would not mean that a circulation model is unnecessary: first, the mixed layer depth is not only a function of local atmospheric forcing but also of current patterns in and below the mixed layer; second, there are areas in the model with significant vertical fluxes across the 100-m level from "horizontal" transports along sloping isopycnals; and third, during summer, the values of temperature, salinity, and nutrient in the layer immediately below the mixed layer but above the depth of maximum winter mixed layer penetration can all be modified through physical transport and mixing, thereby altering the properties of the mixed layer upon reentrainment during autumn and winter.

1976 regime shift

To study the effect of the 1976 regime shift on biological production, we performed simulations with forcing representative of pre- and post-1976 conditions. Here, we identify and compare differences in the physical and biological fields for the pre- and post-1976 simulations with the aim of determining likely causes, and we compare changes that occurred in the model simulations with those determined from observations.

Physical fields

The modelled winter vertically integrated transport stream functions are shown in Fig. 6. The maximum winter integrated transport for the subtropical gyre is about 25% less than the winter Sverdrup transports estimated from wind stress curl maps (from COADS) for the periods 1966–1975 and 1977–1986 by Parrish et al. (2000). However, our model estimates include more dynamical terms, in particular the vorticity sinks associated with the western boundary currents. In Fig. 6, the cyclonic subarctic gyre is roughly twice

Fig. 4. Annual primary production ($\text{mol N}\cdot\text{m}^{-2}\cdot\text{year}^{-1}$) over the top 100 m.

as strong post-1976 relative to pre-1976. This strengthening is due to the intensification of the Aleutian low pressure system leading to an increase in the wind stress curl, which in turn strengthened the gyral circulation. We note, however, a decrease in the (cyclonic) vertically integrated transport stream function in the eastern and northern parts of the Gulf of Alaska. Examining the difference in wind stress between post- and pre-1976, Wu and Hsieh (1999) observed anticyclonic rotation in the Gulf of Alaska, implying a negative wind stress curl leading to a weakening of the gyral circulation.

Changes in the mixed layer depth are shown in Fig. 7. Polovina et al. (1995) calculated winter and spring mixed layer depths from temperature profiles for the North Pacific Ocean ($10\text{--}60^\circ\text{N}$) for the periods 1960–1976 and 1977–1988, and Deser et al. (1996) performed similar calculations for winter mixed layer depths for the periods 1971–1976 and 1977–1988. For most of the subtropical Pacific, they found a deepening of winter and spring mixed layer depths post-1976. Our model results also indicate deepening (Figs. 7a and 7d) throughout the ocean interior (except in summer), which is to be expected both because the increased winter wind stress anticyclonic curl post-1976 would support greater downwelling and because the increased winter wind speeds (fig. 7 in Parrish et al. 2000) would promote deeper mixed layer penetration.

Along the eastern margin, our model predicts that the

mixed layer depth was shallower post-1976 south of 45°N . In the surface forcing fields, the winter SST is warmer in this area (Wu and Hsieh 1999) and the surface water is fresher (Fig. 8), both of which would contribute to a shallowing of the mixed layer depth. In the subarctic Pacific, Freeland et al. (1997) found that salinity must be included to determine interannual changes in the maximum winter mixed layer depth in the subarctic Northeast Pacific. They observed that the midwinter mixed layer depth at OSP (50°N , 145°W) became shallower during the period studied here: 1952–1988. In Fig. 7, OSP, indicated by an asterisk, lies in a (limited) area where the winter mixed layer depth is shallower post-1976 compared with pre-1976, consistent with the results of Freeland et al. (1997).

Biological fields

By examining changes pre- and post-1976 in both the physical fields and the biological fields in the simulations, we can infer the physical mechanisms responsible for the changes in the biological fields. Changes in N are shown in Fig. 9a. In the subtropical gyre, the 1976 regime shift produced stronger zonal winds causing a deepening of the mixed layer (Fig. 7). A deepening of the mixed layer entrains more nutrients into the surface layer, potentially leading to an increase in the concentration of mixed layer N . In the central subarctic Pacific, there is a strengthening of the

Fig. 5. Annual net nitrogen flux ($\text{mol N}\cdot\text{m}^{-2}\cdot\text{year}^{-1}$) across the 100-m level in the (a) advective plus diffusive upward flux of N and (b) downward flux of $P + Z + D$ (mostly sinking particles D).

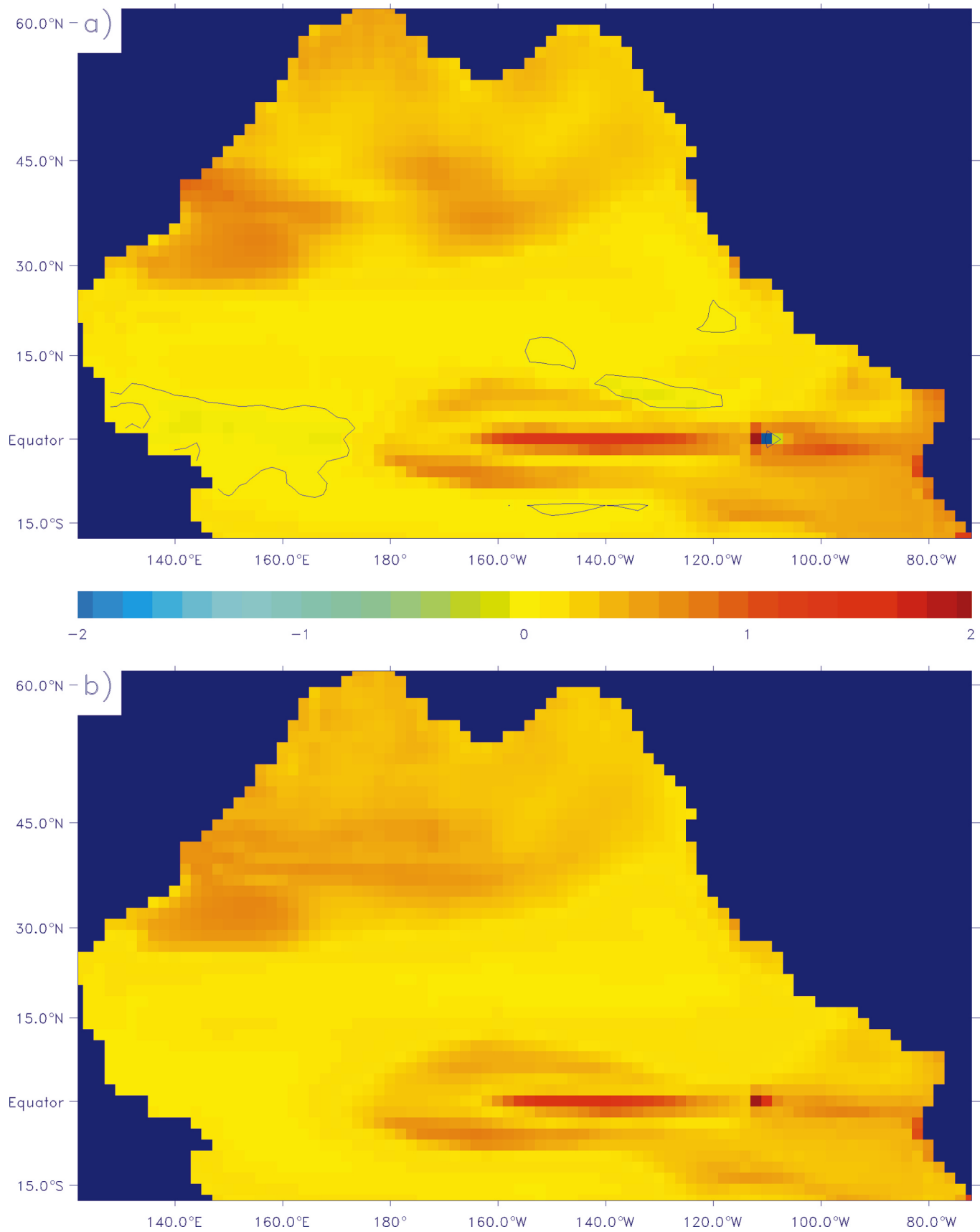
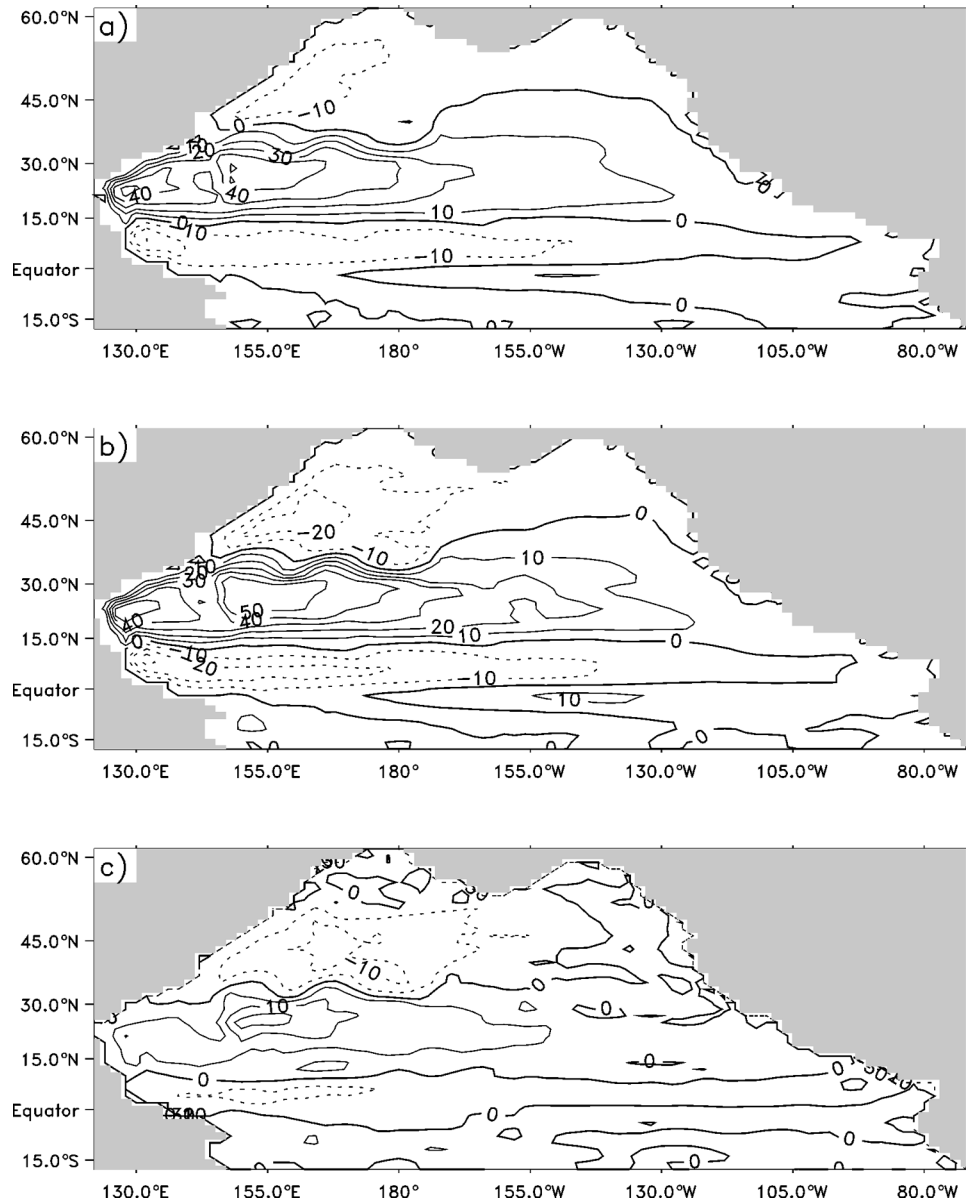


Fig. 6. Winter vertically integrated transport stream function (Sverdrups) (a) from the 1952–1975 baseline run, (b) from the 1977–1988 run, and (c) for post-1976 minus pre-1976. Negative contours denote counterclockwise flow.



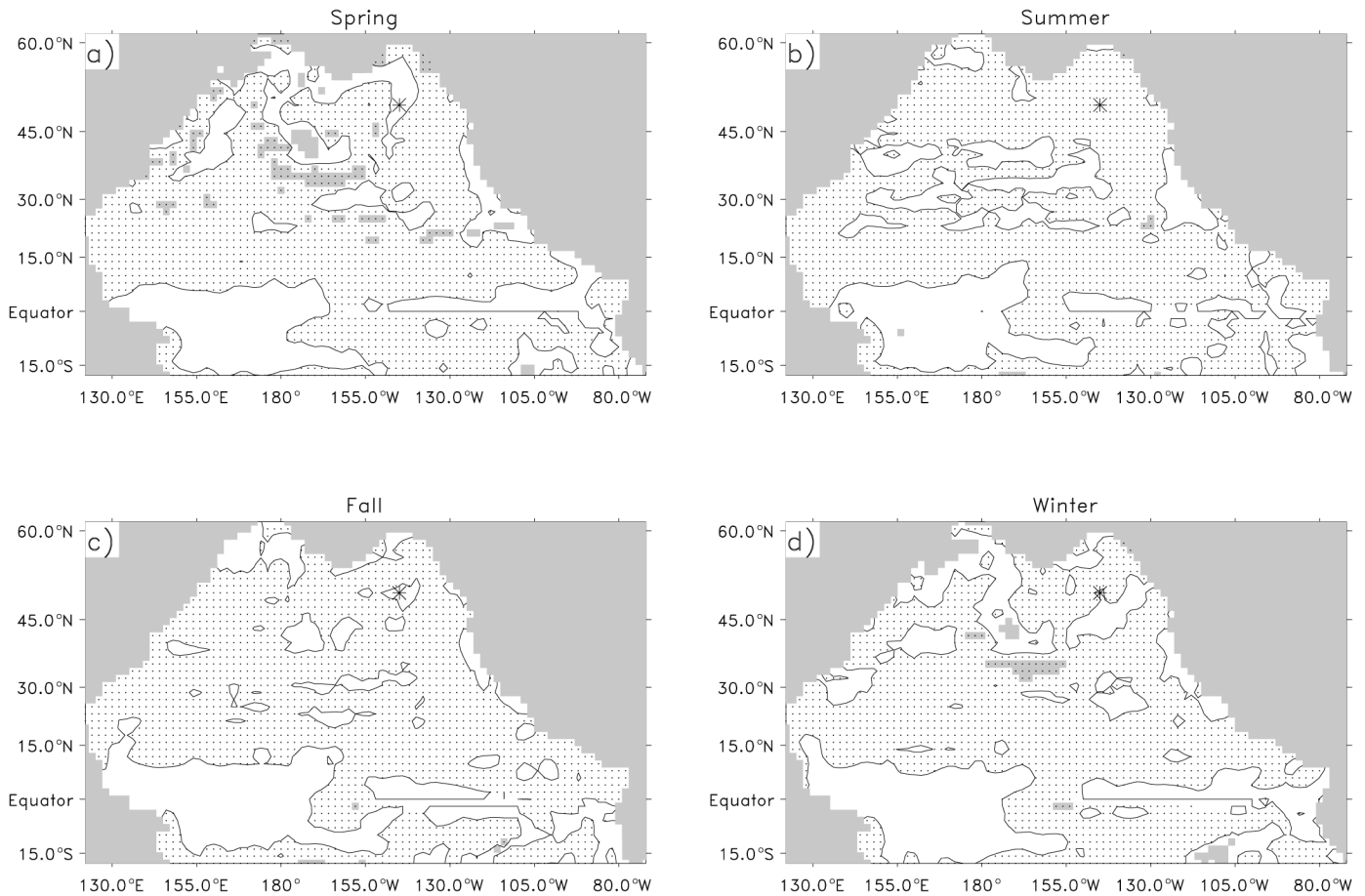
subarctic gyre causing stronger Ekman upwelling, which increases the concentration of mixed layer N but not P (Fig. 9b) because there, N seldom limits primary production. In the subarctic Northeast Pacific, however, there was a weakening of the Alaskan gyre, with weakened Ekman upwelling and hence decreasing N in the mixed layer.

Because the subtropical gyre is broadly nutrient limited, any changes in the macronutrient supply (i.e., N) should have a direct effect on the primary production and concentrations of P (Fig. 9b). Thus, regions with an increase in N show an increase in P , and regions with reduced N show a decrease in P . In particular, there is a band of increased N during winter and spring in the central North Pacific (about 35°N) reflected in a pronounced band of increased P in all seasons, suggestive of a southern shift of both the subarctic front (6° according to Parrish et al. 2000) and the transition zone chlorophyll front. The subarctic gyre, as mentioned in

the previous paragraph, is an area high in macronutrients: changes in the macronutrient supply have little direct effect on primary production. Instead, there exists a correlation between changes in mixed layer depth and changes in phytoplankton biomass P . If the mixed layer is shallower, phytoplankton are exposed on average to more light, and hence, there is more production, as indicated by increased phytoplankton biomass. Similarly, if the mixed layer depth is deeper, then phytoplankton are exposed to less light, leading to a reduction in biomass. Polovina et al. (1995) found a similar relationship between changes in the mixed layer depth and changes in biomass in the subarctic Pacific.

Figure 9c shows changes (post-1976 minus pre-1976) in zooplankton biomass Z , where Z has been integrated down to 100 m to compare with observations, usually obtained from vertical net hauls. The spatial patterns in the seasonal averages of phytoplankton biomass P integrated down to

Fig. 7. Difference in post-1976 and pre-1976 seasonally averaged mixed layer depth. Dotted areas indicate a deeper mixed layer depth post-1976. Contours are of zero change. Shading indicates a greater than 20 m difference. OSP is indicated by an asterisk.



100 m (rather than the mixed layer average shown in Fig. 9b) are similar. Generally, both the *P* and *Z* concentrations increased post-1976 in the subtropical gyre in bands just to the south of the subarctic front and also along the outer margins of the equatorial upwelling tongue, suggesting expansion of these regions into the subtropical gyre.

Venrick et al. (1987) examined chlorophyll *a* trends from 1968 to 1985 in the central North Pacific (26.5–31°N, 150.5–158°W), compiled for the surface 200 m from May to October. For the period between 1968–1973 and 1980–1985, the integrated chlorophyll *a* concentrations through the 5-m stratum containing the maximum concentrations (generally found between 95 and 120 m) increased from 3.32 to 6.50 mg·m⁻², a 96% increase. In the surface 5 m, however, concentrations increased from 1.52 to 1.79 mg·m⁻², only an 18% increase. Averaged over this region for the spring and summer months (March–August), our model predicts a 53% increase in *P* post-1976 over the top 100 m, consistent with the results of Venrick et al. (1987).

Brodeur and Ware (1992) examined the summer (15 June – 31 July) mezozooplankton biomass from net hauls from 150 m to the surface in the Gulf of Alaska (east of 160°W and north of 48°N) for the periods 1956–1962 and 1980–1989. They found up to a twofold increase in zooplankton biomass in the 1980s compared with the late 1950s and early 1960s. Our model does predict an increase in summer zooplankton bio-

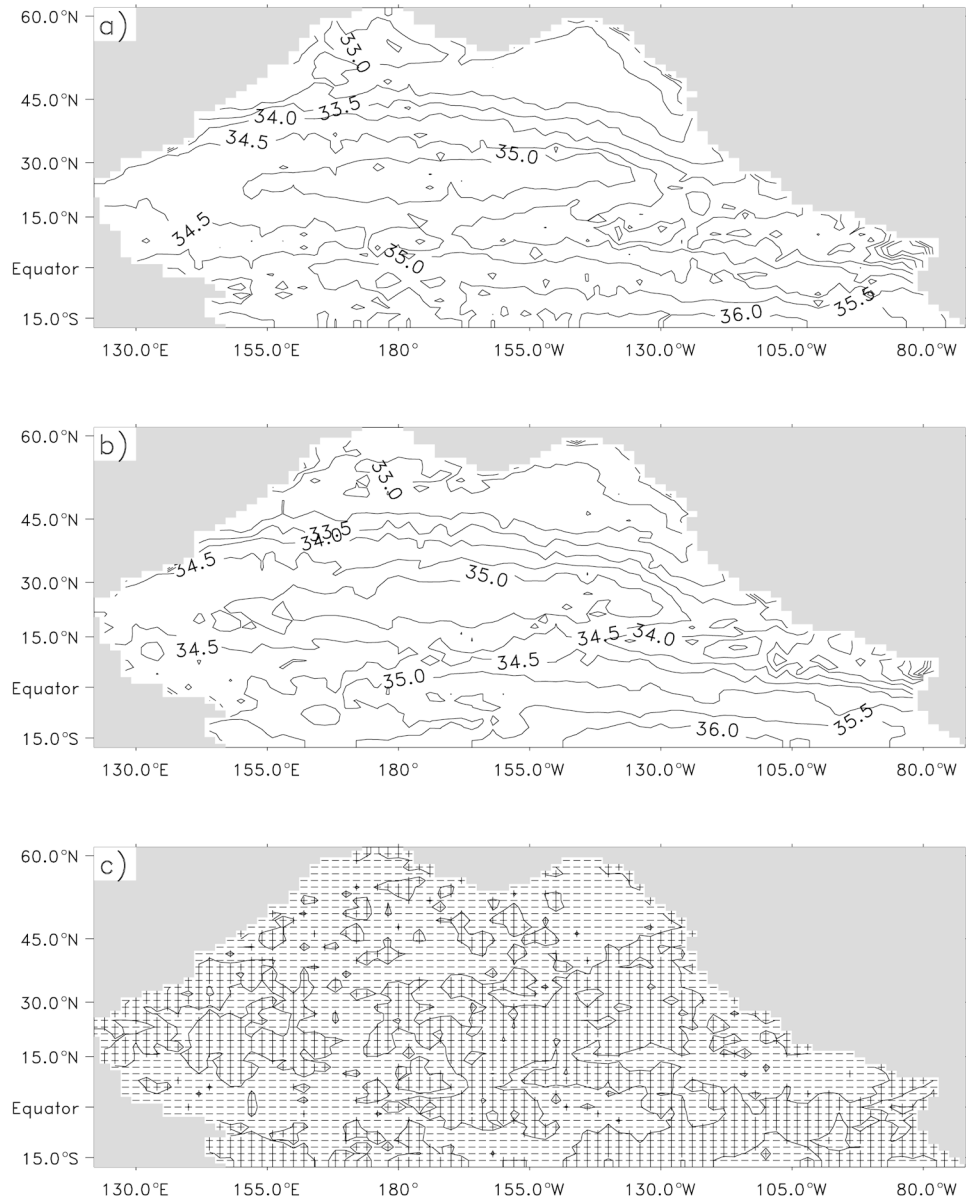
mass (Fig. 9c) as a result of the 1976 regime shift, but the increase (less than 25%) is much smaller. It is difficult to judge how meaningful is this comparison, as Brodeur and Ware's (1992) data do not include the years 1963–1975, which were included in the creation of our pre-1976 climatologies. In addition, we have tuned the zooplankton in our model to represent microzooplankton, which were mostly missed with the mesh sizes of the nets used to obtain the samples reported on by Brodeur and Ware (1992).

Conclusions

The modelled geographic distributions and magnitudes of annual primary production in the baseline run (1952–1988) were within the probable uncertainties of estimates based on observations but biased low compared with estimates based on long-term time series at OSP and station ALOHA. However, the model estimate of export production at OSP was about a factor of 2 too low and at ALOHA was about a factor of 8 less than the most recent published estimates (Karl et al. 1998), suggesting that in the nutrient-limited subtropical gyre, the flux of nutrient into the euphotic layer by the OGCM may be too low. Either the vertical fluxes of nutrients in the OGCM are too low or nutrient inputs by nitrogen-fixing algae (Karl et al. 1997) or from atmospheric deposition (e.g., Duce et al. 1991) may be important.

The forcing fields were then divided into two periods, 1952–

Fig. 8. Climatologies of annually averaged sea surface salinity based on data from WOA98. (a) Climatology for 1952–1975; (b) climatology for 1977–1988; (c) difference between post-1976 and pre-1976 climatologies. In Fig. 8c, a plus sign indicates an increase in sea surface salinity and a minus sign indicates a decrease in sea surface salinity.



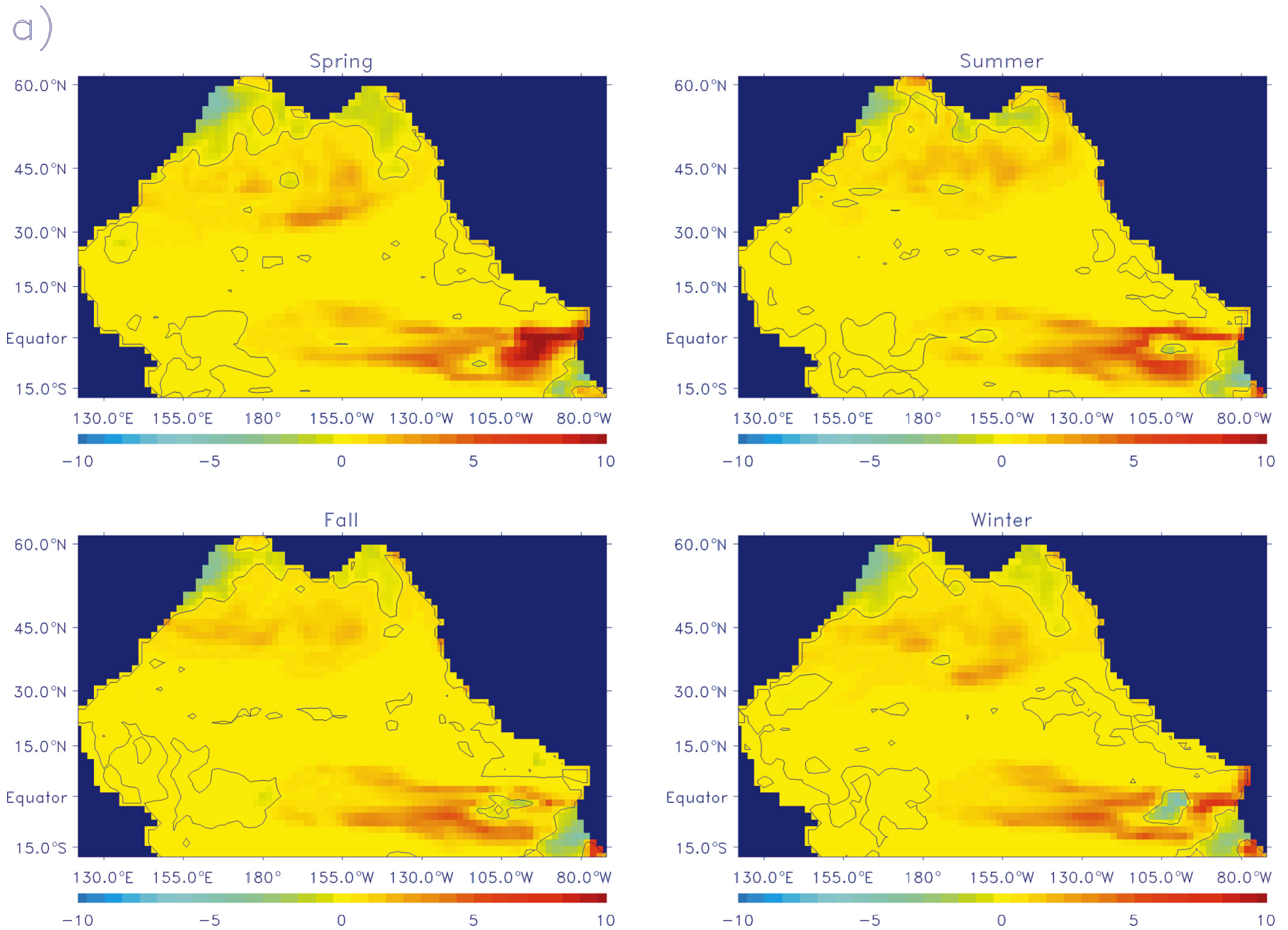
1975 and 1977–1988, to explore the differences in ecosystem responses prior to and after the 1976 climate shift. The simulated wind-driven gyres intensified post-1976 such that the higher production in the subarctic and equatorial zones expanded into the low-production subtropical gyre. In the nutrient-poor subtropical gyre, post-1976 increases in phytoplankton biomass reflected increases in surface layer nutrients. In the HNLC subarctic gyre, phytoplankton biomass increased in regions where the springtime mixed layer depth had shallowed after 1976 such that phytoplankton populations were maintained in higher average light conditions. Changes post-1976 were broadly consistent with observations, but existing observations of changes in nutrients and plankton are inadequate for critical evaluation of the model simulations of the regime shift.

This coupled model is but an initial step towards the more

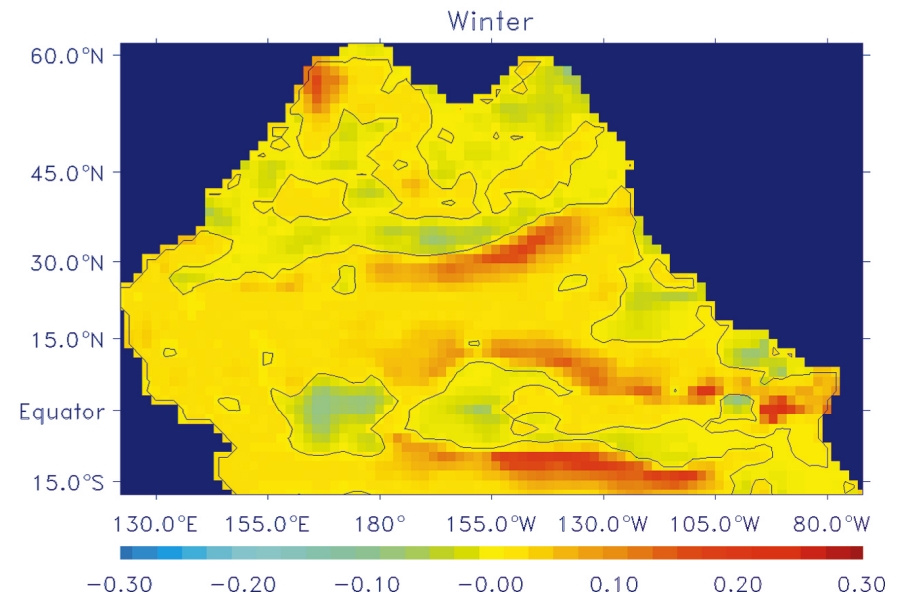
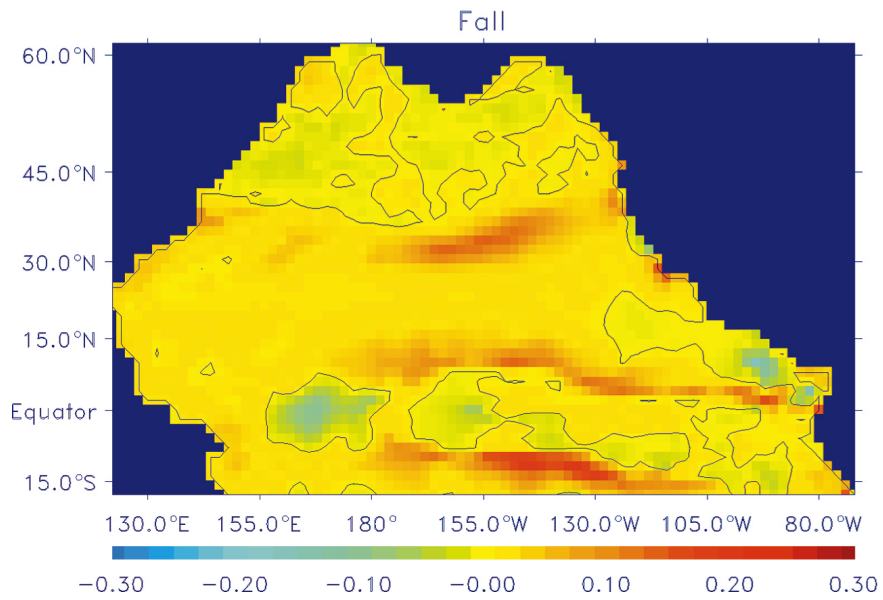
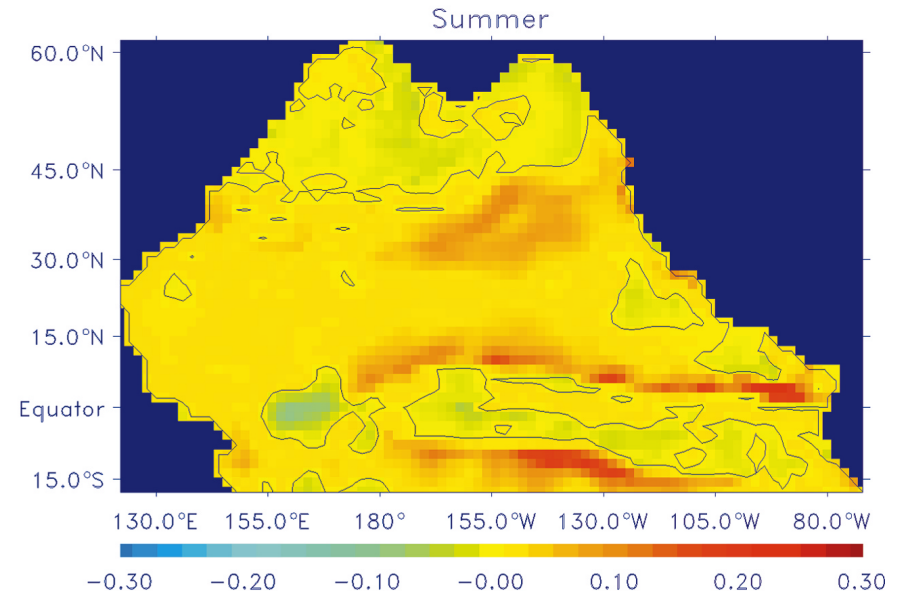
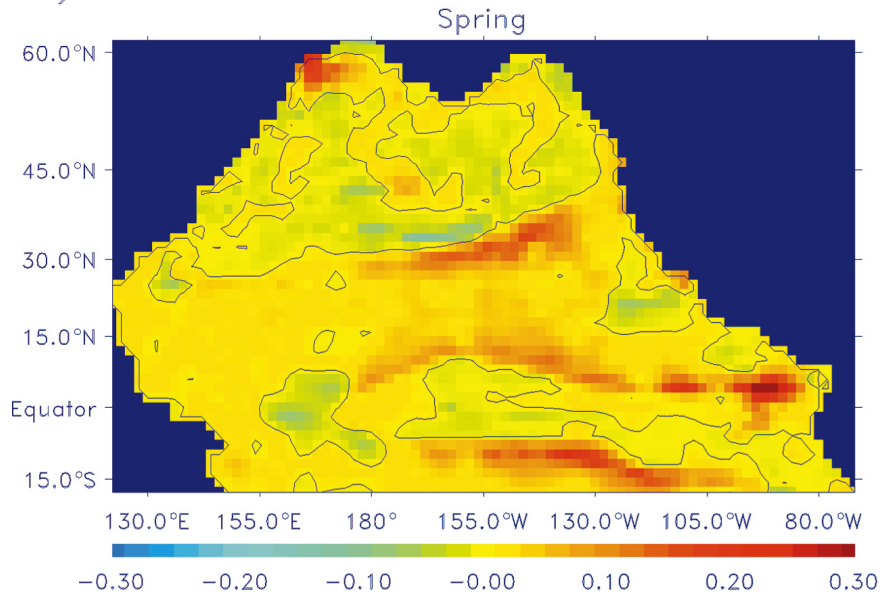
comprehensive coupled models required to investigate pelagic ecosystem responses to climate variation. A key requirement of any OGCM used to drive an open-ocean ecosystem model is that it adequately represents the vertical fluxes of dissolved nutrient into the euphotic zone. We tuned the ecosystem model export production to balance the upward flux of nutrient generated by the physical model, but other studies suggest that at least a factor of 10 improvement in horizontal resolution (in both x and y directions) is required if vertical motions associated with mesoscale eddies are to be accurately represented.

An improved ecosystem model to represent either organic carbon cycling or food web dynamics would need to include partitioning of primary production into at least two phytoplankton groups, microzooplankton, mesozooplankton, and

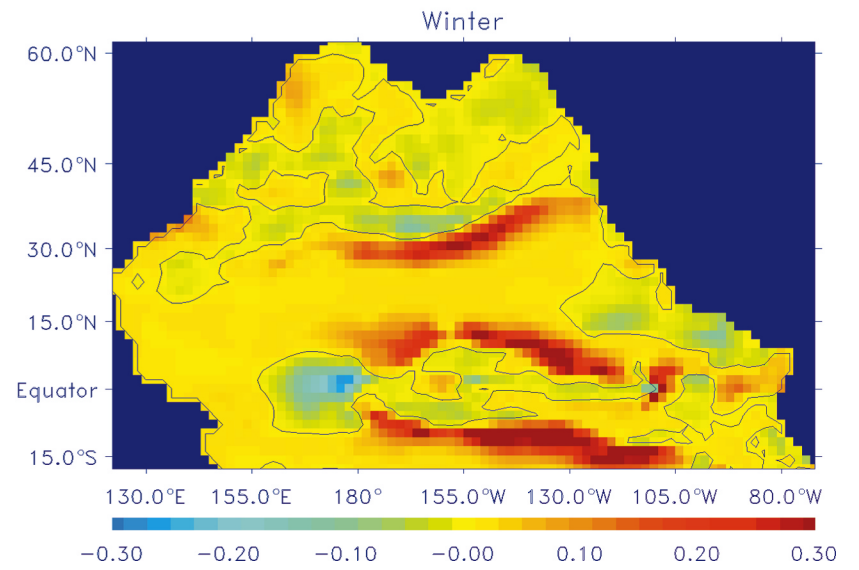
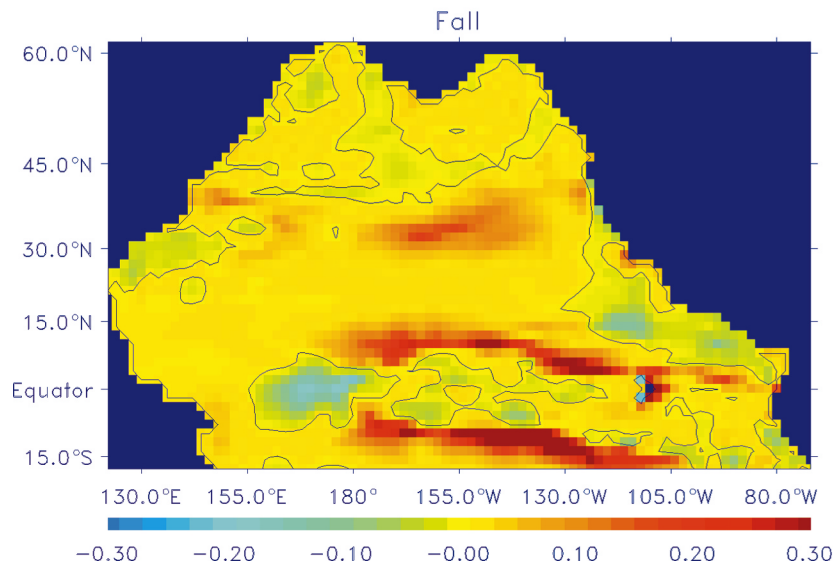
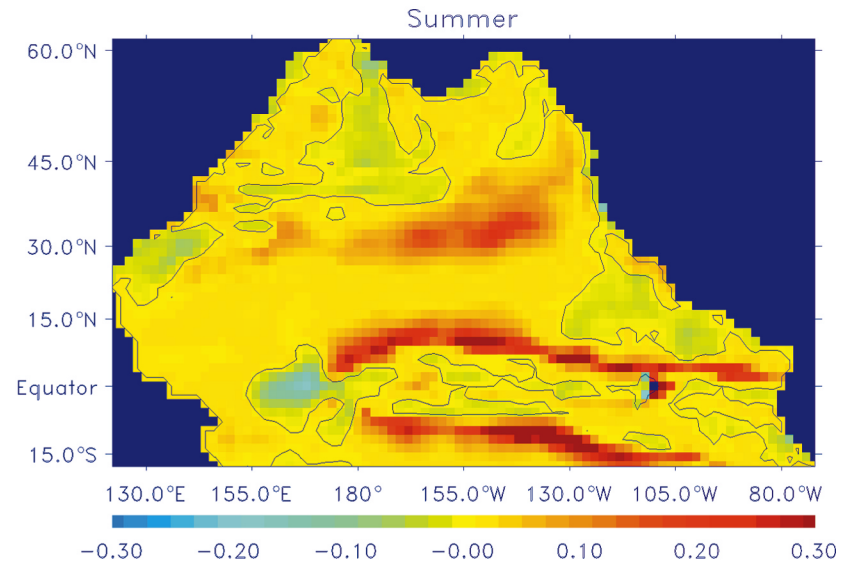
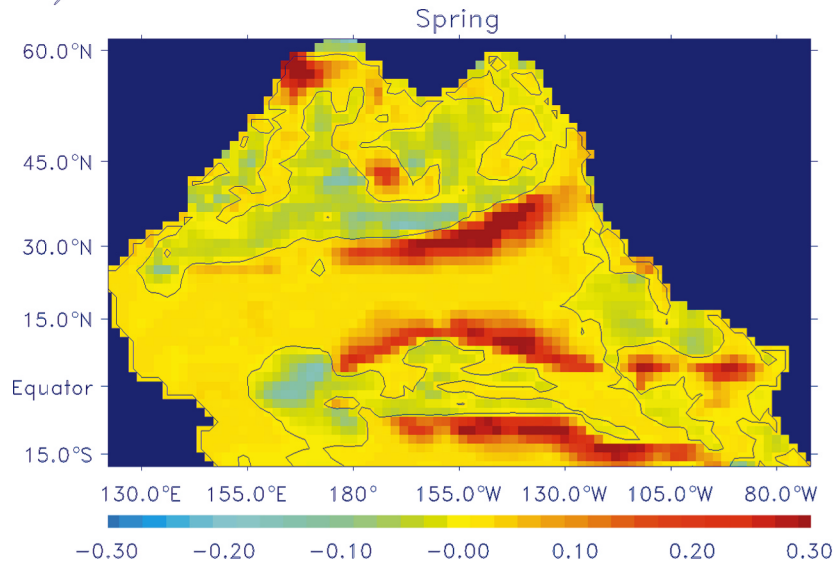
Fig. 9. Seasonal differences between modelled post-1976 and pre-1976 fields. Contours are of zero change. (a) Mixed layer nutrient N concentrations ($\text{mmol N}\cdot\text{m}^{-3}$); (b) mixed layer phytoplankton P concentrations ($\text{mmol N}\cdot\text{m}^{-3}$); (c) microzooplankton Z concentrations ($\text{mmol N}\cdot\text{m}^{-3}$) averaged over the top 100 m.



b)



c)



both dissolved (suspended) and particulate (sinking) organic matter. Even at OSP and ALOHA, both sites of extensive ecosystem and carbon cycling studies in the last decade, more targeted observations are required for the development and critical evaluation of these improved models.

Acknowledgments

We thank Patrick Cummins and Angelica Peña of the Institute of Ocean Sciences for many helpful discussions. Jim Gower of the Institute of Ocean Sciences provided the SeaWiFS data. Reiner Bleck provided the code for MICOM, and S.P.H. benefited from attending annual meetings of the MICOM users group. Alain Vézina and two anonymous referees provided valuable comments on the first submitted manuscript. The project was funded initially by the Meteorological Service of Canada and then by the Natural Sciences and Engineering Research Council and the Department of Fisheries and Oceans as part of the Canadian GLOBEC project.

References

- Beamish, R.J. 1993. Climate and exceptional fish production off the west coast of North America. *Can. J. Fish. Aquat. Sci.* **50**: 2270–2291.
- Beamish, R.J., Noakes, D.J., McFarlane, G.A., Klyashtorin, L., Ivanov, V.V., and Kurashov, V. 1999. The regime concept and natural trends in the production of Pacific salmon. *Can. J. Fish. Aquat. Sci.* **56**: 516–526.
- Bleck, R., Rooth, C., Hu, D., and Smith, L.T. 1992. Salinity-driven thermocline transients in a wind- and thermohaline-forced isopycnic coordinate model of the North Atlantic. *J. Phys. Oceanogr.* **22**: 1486–1505.
- Brodeur, R.D., and Ware, D.M. 1992. Long-term variability in zooplankton biomass in the subarctic Pacific Ocean. *Fish. Oceanogr.* **1**: 32–38.
- Denman, K.L., and Peña, M.A. 1999. A coupled 1-D biological/physical model of the northeast subarctic Pacific Ocean with iron limitation. *Deep-Sea Res. II*, **46**: 2877–2908.
- Denman, K.L., Peña, M.A., and Haigh S.P. 1998. Simulations of marine ecosystem response to climate variation with a one dimensional coupled ecosystem/mixed layer model. *In* Biotic impacts of extratropical climate variability in the Pacific. *Edited by* G. Holloway, P. Müller, and D. Henderson. *Proceedings 1998 'Aha Huliko'a Hawaiian Winter Workshop*, University of Hawaii at Manoa. pp. 141–147.
- Deser, C., Alexander, M.A., and Timlin, M.S. 1996. Upper-ocean thermal variations in the North Pacific during 1970–1991. *J. Clim.* **9**: 1840–1855.
- Drange, H. 1994. An isopycnic coordinate carbon cycle model for the North Atlantic; and the possibility of disposing of fossil fuel CO₂ in the ocean. Ph.D. dissertation, Nansen Environmental and Remote Sensing Center, Solheimsviken, Norway.
- Duce, R.A., Liss, P.S., Merrill, J.T., Atlas, E.L., Buat-Menard, P., Hicks, B.B., Miller, J.M., Prospero, J.M., Arimoto, R., Church, T.M., Ellis, W., Galloway, J.N., Hansen, L., Jickells, T.D., Knap, A.H., Reinhardt, K.H., Schneider, B., Soudine, A., Tokos, J.J., Tsunogai, S., Wollast, R., and Zhou, M. 1991. The atmospheric input of trace species to the world ocean. *Global Biogeochem. Cycles*, **5**: 193–259.
- Emerson, S., Quay, P., Stump, C., Wilbur, D., and Knox, M. 1991. O₂, Ar, N₂, and ²²²Rn in surface waters of the subarctic ocean: net biological O₂ production. *Global Biogeochem. Cycles*, **5**: 49–69.
- Emerson, S., Quay, P., Karl, D., Winn, C., Tupas, L., and Landry, M. 1997. Experimental determination of the organic carbon flux from open-ocean surface waters. *Nature (Lond.)*, **389**: 951–954.
- Evans, G.T., and Parslow, J.S. 1985. A model of annual plankton cycles. *Biol. Oceanogr.* **3**: 327–347.
- Falkowski, P.G., and Wilson, C. 1992. Phytoplankton productivity in the North Pacific Ocean since 1900 and implications for absorption of anthropogenic CO₂. *Nature (Lond.)*, **358**: 741–743.
- Fasham, M.J.R. 1995. Variations in the seasonal cycle of biological production in subarctic oceans: a model sensitivity analysis. *Deep-Sea Res. I*, **42**: 1111–1149.
- Francis, R.C., Hare, S.R., Hollowed, A.B., and Wooster, W.S. 1998. Effects of interdecadal climate variability on the oceanic ecosystems of the NE Pacific. *Fish. Oceanogr.* **7**: 1–21.
- Freeland, H., Denman, K., Wong, C.S., Whitney, F., and Jacques, R. 1997. Evidence of change in the winter mixed layer in the Northeast Pacific Ocean. *Deep-Sea Res. I*, **44**: 2117–2129.
- Gargett, A.E. 1984. Vertical eddy diffusivity in the ocean interior. *J. Mar. Res.* **42**: 359–393.
- Gaspar, P., Gregoris, Y., and Lefevre, J.M. 1990. A simple eddy kinetic energy model for simulations of the oceanic vertical mixing: test at station papa and the long term upper ocean study site. *J. Geophys. Res.* **95**: 16 179 – 16 193.
- Goericke, R., and Montoya, J.P. 1998. Estimating the contribution of microalgal taxa to chlorophyll *a* in the field — variations of pigment ratios under nutrient- and light-limited growth. *Mar. Ecol. Prog. Ser.* **169**: 97–112.
- Hanawa, K., Yoshikawa, Y., and Watanabe, T. 1989. Composite analyses of wintertime wind stress vector fields with respect to SST anomalies in the western North Pacific and the ENSO events: Part I. SST composite. *J. Meteorol. Soc. Jpn.* **67**: 385–400.
- Harrison, P.J., Boyd, P.W., Varela, D.E., Takeda, S., Shiimoto, A., and Odate, T. 1999. Comparison of factors controlling phytoplankton productivity in the NE and NW subarctic Pacific gyres. *Prog. Oceanogr.* **43**: 205–234.
- Iqbal, M. 1983. *Introduction to solar radiation*. Academic Press, Toronto, Ont.
- Karl, D., Letelier, R., Tupas, L., Dore, J., Christian, J., and Hebel, D. 1997. The role of nitrogen fixation in biogeochemical cycling in the subtropical North Pacific Ocean. *Nature (Lond.)*, **388**: 533–538.
- Karl, D.M., Hebel, D.V., and Björkman, K. 1998. The role of dissolved organic matter release in the productivity of the oligotrophic North Pacific Ocean. *Limnol. Oceanogr.* **43**: 1270–1286.
- Landry, M.R., Barber, R.T., Bidigare, R.R., Chai, F., Coale, K.H., Dam, H.G., Lewis, M.R., Lindley, S.T., McCarthy, J.J., Roman, M.R., Stoecker, D.K., Verity, P.G., and White, J.R. 1997. Iron and grazing constraints on primary production in the central equatorial Pacific: an EqPac synthesis. *Limnol. Oceanogr.* **42**: 405–418.
- Large, W.G., and Pond, S. 1981. Open ocean momentum flux measurements in moderate to strong winds. *J. Phys. Oceanogr.* **11**: 324–336.
- Levitus, S., Boyer, T.P., Conkright, M.E., O'Brien, T., Antonov, J., Stephens, C., Stathoplos, L., Johnson, D., and Gelfeld, R. 1998. NOAA Atlas NESDIS 18, World Ocean Database 1998. Vol. 1. Introduction. U.S. Government Printing Office, Washington, D.C.
- McDougall, T.J., and Dewar, W.K. 1998. Vertical mixing and cabelling in layered models. *J. Phys. Oceanogr.* **28**: 1458–1480.
- Miller, A.J., and Schneider, N. 2000. Interdecadal climate regime dynamics in the North Pacific Ocean: theories, observations and ecosystem impacts. *Prog. Oceanogr.* **47**: 355–379.

- Mysak, L.A. 1986. El Niño, interannual variability and fisheries in the northeast Pacific Ocean. *Can. J. Fish. Aquat. Sci.* **43**: 464–497.
- Nakamura, H., Lin, G., and Yamagata, T. 1997. Decadal climate variability in the North Pacific during the recent decades. *Bull. Am. Meteorol. Soc.* **78**: 2215–2225.
- Parrish, R.H., Schwing, F.B., and Mendelssohn, R. 2000. Mid-latitude wind stress: the energy source for climatic shifts in the North Pacific Ocean. *Fish. Oceanogr.* **9**: 224–238.
- Polovina, J.J., Mitchum, G.T., and Evans, G.T. 1995. Decadal and basin-scale variation in mixed layer depth and the impact on biological production in the Central and North Pacific, 1960–88. *Deep-Sea Res. I*, **42**: 1701–1716.
- Strom, S.L., Postel, J.R., and Booth, B.C. 1993. Abundance, variability, and potential grazing impact of planktonic ciliates in the open subarctic Pacific Ocean. *Prog. Oceanogr.* **32**: 185–203.
- Sugimoto, T., and Tadokoro, K. 1997. Interannual–interdecadal variations in zooplankton biomass, chlorophyll concentration and physical environment in the subarctic Pacific and Bering Sea. *Fish. Oceanogr.* **6**: 74–93.
- Trenberth, K.E., and Hurrell, J.W. 1994. Decadal atmosphere–ocean variations in the Pacific. *Clim. Dyn.* **9**: 303–319.
- Trenberth, K.E., Large, W.G., and Olson, J.G. 1989. The effective drag coefficient for evaluation of wind stress over the oceans. *J. Clim.* **2**: 1507–1516.
- Varela, D.E., and Harrison, P.J. 1999. Seasonal variability in the nitrogenous nutrition of phytoplankton in the northeastern subarctic Pacific Ocean. *Deep-Sea Res. II*, **46**: 2505–2538.
- Venrick, E.L., McGowan, J.A., Cayan, D.R., and Hayward, T.L. 1987. Climate and chlorophyll *a*: longterm trends in the central North Pacific Ocean. *Science (Washington, D.C.)*, **238**: 70–72.
- Webb, W.L., Newton, M., and Starr, D. 1974. Carbon dioxide exchange of *Alnus rubra*: a mathematical model. *Ecologia*, **17**: 281–291.
- Woodruff, S.D., Slutz, R.J., Jenne, R.L., and Steurer, P.M. 1987. A comprehensive ocean–atmosphere data set. *Bull. Am. Meteorol. Soc.*, **68**: 1239–1250.
- World Ocean Atlas. 1994. CD-ROM data set documentation. Tech. Rep., National Oceanography Data Center, Ocean Climate Laboratory, U.S. Department of Commerce, NOAA, National Environmental Satellite Data and Information Service, Washington, D.C.
- Wu, J.Q., and Hsieh, W.W. 1999. A modelling study of the 1976 climate regime shift in the North Pacific Ocean. *Can. J. Fish. Aquat. Sci.* **56**: 2450–2462.